Scientific report; WR 99 - 03

KNMI

The KNMI Gardren Experiment: micro-meteorological observations 1988-1989

corrections

Fred C. Bosveld

De Bilt, 1999

Scientific report = wetenschappelijk rapport; WR 99 - 03

De Bilt, 1999

PO Box 201
3730 AE De Bilt
Wilhelminalaan 10
De Bilt
The Netherlands
Telephone + 31(0)30-220 69 11
Telefax + 31 (0)30-221 04 07

Author: Fred C. Bosveld

UDC: 551.506.24
551.584.41
551.501
(492)

ISSN: 0169-1651

ISBN: 90-369-2163-5

The KNMI Garderen Experiment,

Micro-meteorological observations 1988-1989.

Corrections

Fred C. Bosveld

Contents

1 Introduction

During the period 1988-1989 KNMI has run a forest micro-meteorological research site at the Speulderbos near the small town of Garderen, The Netherlands. The measurements were performed in the context of ACIFORN (Acidification of Forests in the Netherlands) a sub-project of the Dutch Additional Programme on Acidification. Measurements were performed along a 36 m tall open structured mast. They include: a) profile measurements of wind, dry-bulb temperature and wet-bulb temperature, b) fast response turbulence measurements of wind, temperature and humidity and c) shortwave incoming radiation, net radiation and infrared radiation temperature. Details on the site and the measuring program are described in Bosveld et al. (1998). This report deals with various corrections which are performed on the data.

Outdoor measurements of meteorological variables are always prone to uncertainties. An important difference with the laboratory situation is that outdoor experiments can not be repeated under the same conditions. Therefore it is of importance to check instrumental performance at the time of the experiment. This can be achieved by on-line data output. To perform quality checks it is of importance to have some kind of redundancy in the measurements. Despite the best efforts one is at times confronted with instrumental problems in the data only after the experiment, at the time that a more thorough data analysis is performed. This problems can be called the nightmare of the instrumentalist.

A number of sources of uncertainties can be discriminated. Uncertainties arise because of the inherent statistical nature of atmospheric turbulence. This aspect is thoroughly described in the literature (Lumley and Panofsky, 1964) and will not be treated further here. Uncertainties arise because instruments often do not measure exactly the variable that we need. For example instruments that measure turbulent fluctuations have limited response at the high frequency side of the spectrum. Often data can be corrected for this kind of uncertainties within certain limits. Other uncertainties arise because of mall-functioning of instruments. In the best case one may discover the source of mall-functioning and prove that the error is reproducible and can be quantified. If this is not the case one is probably able to estimate the magnitude of the uncertainty. One is then left with data that are more uncertain then intended, and one may hope that objectives of the investigation can still be met. If none of this is the case one can only reject the data.

Some straightforward data checks and corrections are described in a separate technical report (Bosveld et al., 1998). They include treatment of cup anemometer calibrations, an in situ calibration of the Ly-α fluctuation hygrometer, offset and drift in the observations of dry- and wet bulb temperature differences and calibration of the sonical temperature. In this report we concentrate on more complex corrections. They involve two 'nightmares of the experimentalist'. One is related to a tilted net radiometer described in Chapter 2, the other is related to a mall-functioning D/A-converter in the wind unit of the sonic anemometer described in Chapter 7. In Chapter 3 the theory of the structure parameter of the wind is treated. It proves to be an interesting quantity in its own right because it gives direct information on the structure of inertial subrange turbulence. Moreover, it can be used to quantify various instrumental uncertainties especially, those that are related to limited response at the high frequency end of the spectrum. Chapters 4 is devoted to the the measurement problems of the structure parameter of the wind. Related to this is Chapter 5 on the influence of line averaging on eddy-correlation observations and Chapter 11 on cup-anemometer overspeeding, including an experimental verification of overspeeding. The short Chapter 10 gives an indication of mast interference with wind speed measurements. Chapter 8 treats the calibration of the sonic anemometer. A procedure is derived to correct the instrument for

transducer shadow effects. Chapter 6 treats the problem of low frequency loss in eddy-covariance measurements, due to finite averaging time. Were possible use is made of the redundancy in the data to check on the correctness of the various corrections applied. This dictates the sequence of corrections and determines, at least partly, the order in which the various topics are described in this report.

2 Errors in the net radiation measurements

2.1 Introduction

Net radiation measurements are known to be susceptible to a number of errors (Halldin et al., 1992). Of these the most notable are: difference between calibration conditions and field conditions, differences in sensitivity to short wave radiation and long wave radiation, sensitivity to aging of the dooms, difference in radiation properties of the supporting mast compared to the surface and sensitivity to tilt in particular when the direct sunlight component is large. For the current data-set two problems were especially important.

A systematic underestimation of net radiation (Q) of 8% was found. For specially selected overcast cases an independent estimation of net radiation was obtained. Observed short wave incoming radiation together with an estimated albedo of 0.10 was used. Net long wave cooling was assumed to be small and constant over the day for these selected cases. Accuracy of the Kipp pyranometer, with which short wave incoming radiation is measured, is well established making it likely that the net radiometer was in error. For other experiments comparable deviations were found for the the Funk-type net radiometers used at KNMI. This led to an investigation of the KNMI calibration standard for net radiation. Kohsiek (1996) compared a pyranometer with the net radiometer used as a calibration standard at KNMI. He found by comparing the responses during a shadowing experiment during a clearsky day that the standard underestimated short wave radiation by 6%. All net radiation data were corrected accordingly. The remaining discrepancy of 2% might well come from aging of the domes during the one month interval between replacement of the domes.

The second problem relates to a tilt of the net-radiometer of several degrees out of the horizontal plane. The main part of this appendix is devoted to developing a correction procedure for this error.

2.2 Correcting a tilted net radiation sensor

The Funk net radiation meter is mounted on a boom that can be rotated to the mast in the horizontal plane for maintenance purposes. The instrument was levelled when the boom was rotated inward. In the course of the experiment it was realised that the rotation axis of the boom was not strictly vertical. The error in Q due to a tilting of the instrument is almost entirely attributable to the effect on the direct shortwave radiation. The diffusive radiation components does not contribute significantly to this error. Let θ_i be the tilting angle of the instrument then for homogeneous diffuse light it can be shown that the measured net radiation is $\cos(\theta_i)$ times the actual net radiation. For a tilt of 5° this result in a deviation of 0.5%.

The direct sunbeam gives rise to a larger error in the net radiation. Let K_{dir} be the direct short wave flux density perpendicular to the beam then the error can be written as:

$$\delta Q = K_{dir} \left(\vec{e}_z - \vec{e}_i\right)\cdot\vec{e}_S \qquad (2.1)$$

where, $\vec{e}_Z$ is the unit vector perpendicular to the horizontal plane, $\vec{e}_i$ the unit vector perpendicular to the surface of the instrument and $\vec{e}_S$ the unit vector parallel to the sunbeam. Let h be the elevation of the sun above the horizon and φ_s the azimuth relative to north (positive over east). Finally let φ_i be the azimuth of direction of tilt. In terms of these angles and retaining only first

order terms in θ_i equation (2.1) results in:

$$\delta Q = -\theta_i K_{dir} \cos(\phi_i - \phi_S) \cos(h) \tag{2.2}$$

For the estimation of direct solar radiation we use the algorithm derived by De Jong (1980) (see also Velds, 1992). This algorithm gives an estimate of diffuse solar radiation as function of time averaged global radiation. The algorithm is tested on a data set obtained in De Bilt, the Netherland. Here we modify this algorithm for the use of direct solar radiation. The global radiation is split in its diffuse and direct component:

$$K^{\downarrow} = K_{dir} \sin(h) + K_{dif} \tag{2.3}$$

The extra-terrestrial values of $K^{\downarrow}$ and K_{dir} are K_0 and I_0 respectively where $K_0 = I_0 \bullet \sin(h)$. I_0 is the solar constant and varies only a few percent throughout the year due to variation in the distance of the earth to the sun. The 'De Jong' algorithm then relates the ratio $K^{\downarrow}/K_0$ to the ratio K_{dir}/I_0. Table 2.a summarises the algorithm. The accuracy is circa 100 W m^{-2}.

To estimate tilt angle and tilt azimuth from the observed net radiation we need an independent estimate for the net radiation. Since not all the components of the radiation balance are measured we have to rely on some parameterisation of terms in the radiation balance. The radiation balance or net radiation Q_{net} is given by:

$$Q = K^{\downarrow} - K^{\uparrow} + L^{\downarrow} - L\uparrow \tag{2.4}$$

where $K^{\downarrow}$ is the short wave incoming radiation, $K^{\uparrow}$ short wave outgoing radiation, $L^{\downarrow}$ long wave incoming radiation and $L^{\uparrow}$ the long wave outgoing radiation. Of this components short wave incoming radiation is measured and the infrared radiation temperature of the forest is measured from which the long wave outgoing radiation can be derived.

Short wave outgoing radiation is parameterised with an albedo of 0.10. For the downward longwave radiation we rely on a model for cloud free conditions given by Brutsaert (1975) which relates $L^{\downarrow}$ to T_a and e_a the temperature and water vapour pressure at screen level:

$$L^{\downarrow} = 1.24 \left(\frac{e_a}{T_a} \right)^{1/7} \sigma T_a^4 \tag{2.5}$$

For cloudy skies the situation is more complicated. Cloud base temperature and cloud cover fraction becomes important. Thus we limit to clear sky conditions. We are now in a position to derive an independent estimate of the net radiation for clearsky conditions in terms of measured quantities:

$K^{\downarrow}/K_0$	K_{dir}/I_0
< 0.22	0
0.22 - 0.35	$6.4 \bullet (X-0.22)^2$
0.35 - (1.47-R)/1.66	$(1.6 \bullet X-0.47)$
> (1.47-R)/1.66	R

$X = K^{\downarrow}/K_0$ and $R = 0.847 - 1.61 \sin(h) + 1.04 \sin^2(h)$

Table 2.a Algorithm to derive direct sunlight form global radiation observations.

$$Q_{\text{mod}} = (1-r)\ K^{\downarrow} + 1.24 \left(\frac{e_a}{T_a}\right)^{1/7} \sigma T_a^4 - \sigma T_s^4 \qquad (2.6)$$

Figure 2.1 shows results for one clearsky day. Figure 2.1a shows the observed net radiation and short wave incoming radiation together with the modelled net radiation and a modelled short wave incoming clearsky radiation $K^{\downarrow}$(mod) with low atmospheric water content and low turbidity according to Raaf (1987). It is observed that global radiation is relatively low indicating high turbidity and thus relatively low direct solar radiation. Figure 2.1b gives for an eye fitted tilt and azimuth of tilt the estimated deviation in the net radiation. A line is drawn for the modelled deviation. Furthermore the difference between observed and modelled net radiation are displayed before and after correction for this tilt. The eye-fitt tilt and azimuth is obtained by varying tilt and azimuth of the model net radiometer such that a good correspondence is obtained between the modelled (with De Jong direct solar radiation) and the observed deviation. All days with a clearsky period of at least several hours were investigated resulting in a series of tilt and azimuth values throughout the year. It appeared that these values stayed approximately constant within periods where no handling with the instrument occurred. For each period with no instrument handling a tilt and azimuth was determined. Corrections were performed accordingly.

2.3 Radiation influence of the mast.

Here we investigate the influence of the supporting mast on the net radiation instrument. The instrument is mounted on a 2.5m long boom which itself stick horizontally out of the top of the mast in the direction 120° relative to North, positive over East. The mast itself has a triangular base with sides of 1.2m. It can be shown that for a isotropic diffuse radiance, homogeneous distributed over the side of the mast, the relative contribution of the mast to the radiation measurement is $d/(2\pi b)$, where d is the width of the mast and b is the length of the boom. This amounts to a fraction 0.1. As an order of magnitude estimate let us assume that the irradiation on the mast side is equal to the shortwave incoming radiation. Let us further assume a transparency of the construction of 0.5 and an albedo of 0.5, whereas the albedo of the vegetation is circa 0.10. As an order of magnitude we have that a fraction 0.05 of the radiation field is increased with 0.4 times the global radiation. Thus an extra 2% of the global radiation is added to the upward shortwave radiation. It must be noted that for low solar elevation in the morning the contribution can be higher especially when turbidity is low and thus direct solar radiation is high. Figure 2.2 shows comparable graphs as Figure 2.1 but now for a day with high direct solar radiation. It is observed that after tilt correction a deviation of maximal 30 W m^{-2} remain. This is most likely caused by mast interference. No correction is performed for this mast radiation effect.

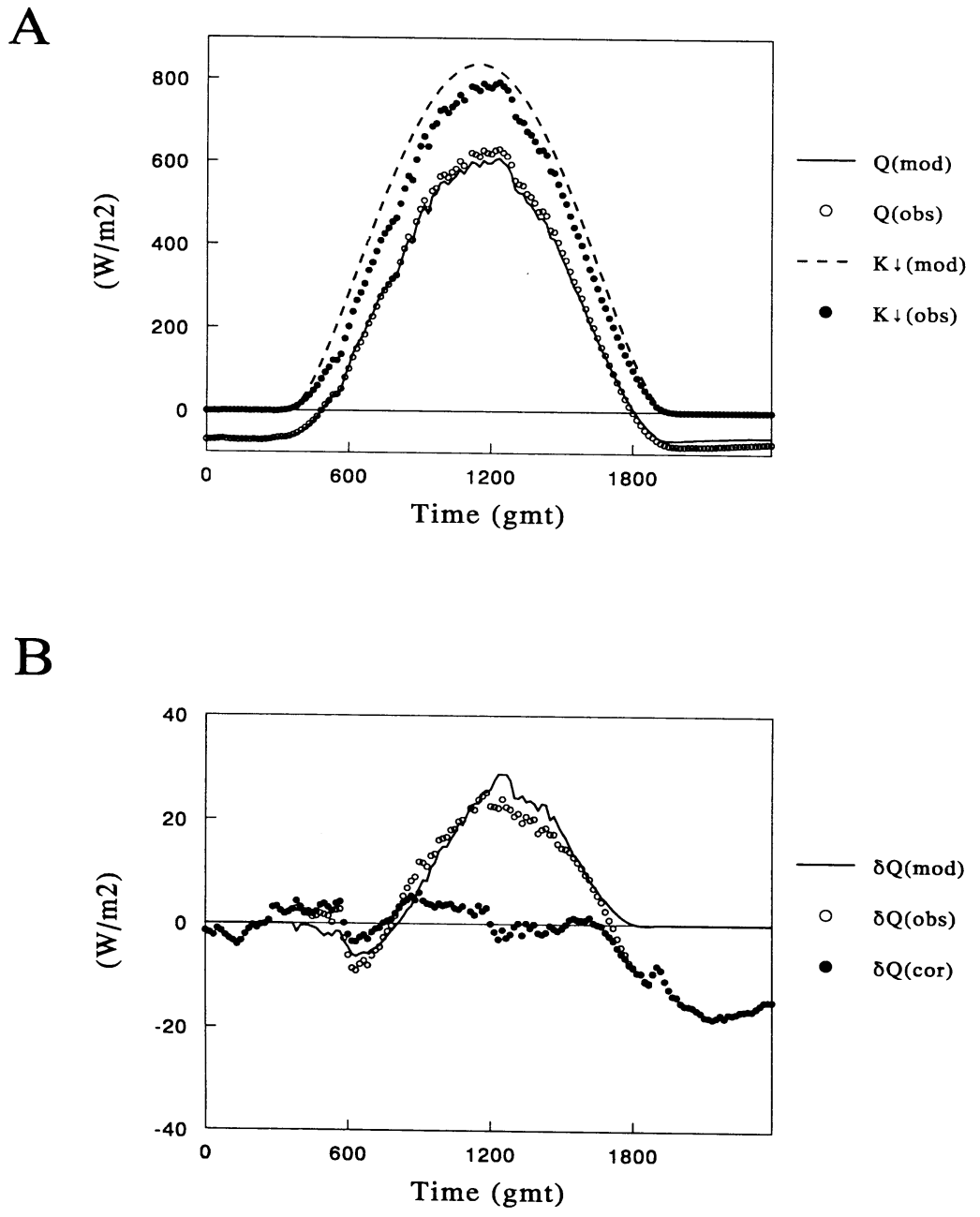

Figure 2.1 Departure in net radiation due to tilt for a clear day with high turbidity. A) Observed and modelled radiation components together with the clearsky short wave radiation of Raaff, B) deviations

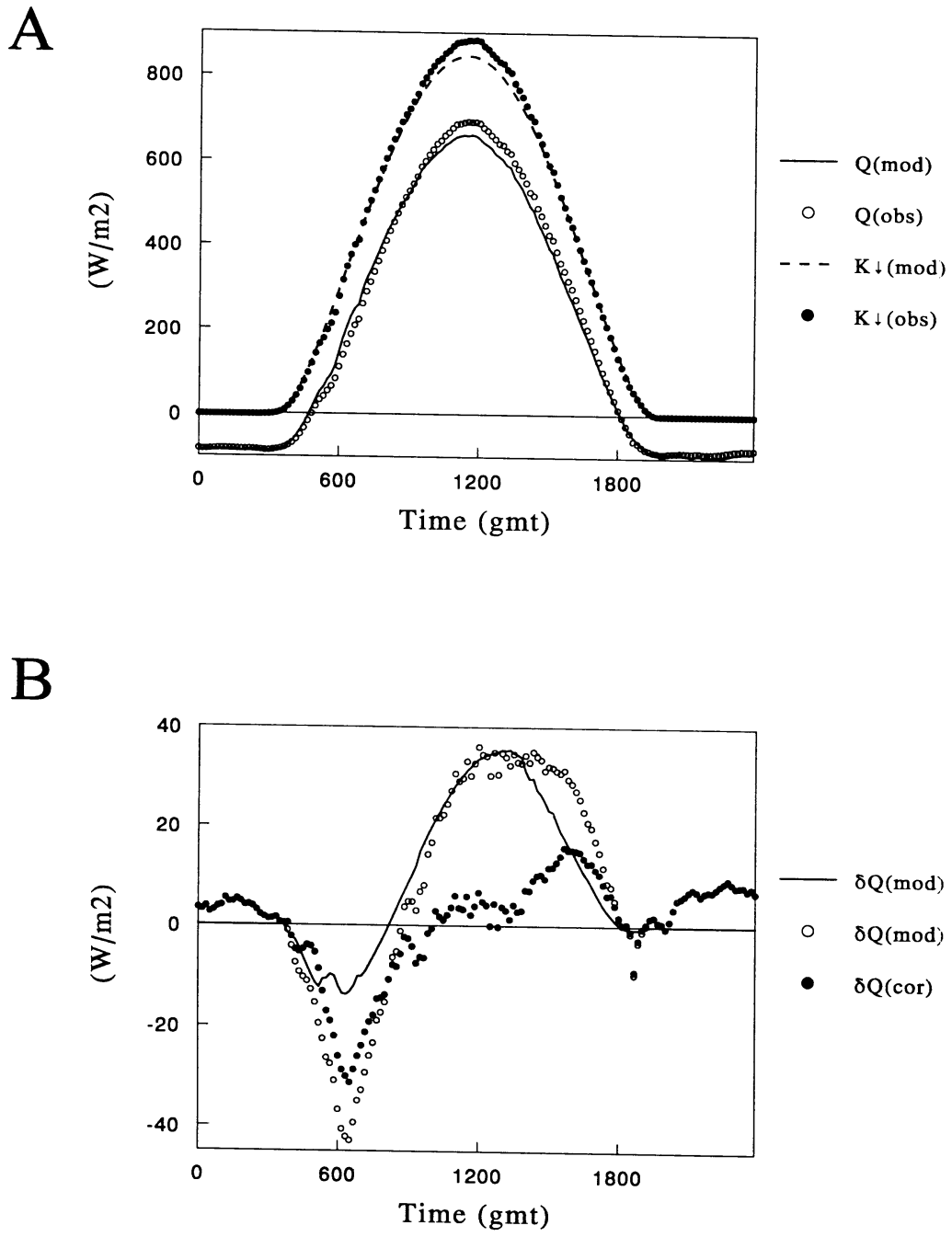

Figure 2.2 Indication of mast reflection. As figure 2.1 but for a low turbidity clearsky day.

3 The structure parameters of the wind.

3.1 Introduction

Structure parameters and the closely related structure functions are convenient quantities to obtain statistical information about the smaller scales of turbulent quantities. Temperature and moisture structure parameters are used in describing propagation of electromagnetic waves (Tatarski, 1967) and acoustic waves through the atmosphere (Weil, 1991). In micro-meteorology they are used to derive surface fluxes indirectly with Monin-Obhukov similarity relations (Kohsiek, 1982; Kohsiek and Bosveld, 1987; Fairall et al., 1990). Structure parameters of wind can be used obtain indirect estimates of momentum transport and dissipation of turbulent kinetic energy by assuming the presence of an inertial subrange in the kinetic energy spectrum. One could say that the use of structure parameters in micro-meteorological practice is a convenient way to get some spectral information. The measurements can easily be processed on-line to average values over a desirable time interval.

There are two fundamental interpretation problems with structure parameters, one related to the Taylor hypothesis used to transform from the time domain to the spatial domain, and one related to the increased intermittency on smaller scales of the dissipation. These will be treated in this appendix. Measurements of structure parameters in the atmospheric surface layer sets high demands on the spatial and temporal resolution of the instruments. If this demand are not satisfied important corrections have to be applied for spectral loss. This is the topic of the next appendix.

3.2 Definition of the structure function for wind

For horizontal homogeneous conditions the structure function of a velocity component A along an arbitrary direction in space is defined as:

$$D_a^2(x) = \left\langle \left(a(y+x)-a(y)\right)^2 \right\rangle \tag{3.1}$$

where the brackets denote averaging over a horizontal surface, y is some position in space and x is the separation in space. a denotes the fluctuation of A around its average value $\langle A \rangle$. The structure function relates to the autocorrelation function R_{aa} according to:

$$R_{aa}(x) = \langle a(y+x)\cdot a(y) \rangle = R_{aa}(0) - \frac{1}{2}D_a^2(x) \tag{3.2}$$

where $R_{aa}(0)$ is the variance of a.

For spatial separations x in the inertial subrange, i.e. x much smaller then the scale L on which energy is produced and much larger then the viscous length scale η, a scaling law for D_a^2 can be derived by observing that the only physical relevant scales are the energy dissipation rate ε and the spatial separation x itself. From this we conclude on dimensional grounds that:

$$D_a^2(x) \sim (\varepsilon \cdot x)^{2/3} \tag{3.3}$$

The structure parameter of the windcomponent A is defined by:

$$C_a^2(x) = D_a^2(x)\, x^{-2/3} \sim \varepsilon^{2/3} \tag{3.4}$$

In the inertial subrange we may expect C_a^2 to be independent of x and according to Equation (3.3)

to be proportional to $2/3^{th}$ power of the dissipation rate. Moreover when the condition of isotropy is satisfied the constant of proportionality only depends on the angle between the average windvector and the direction along which the wind component is measured.

3.3 Converting from time coordinates to space coordinates

In practice we measure a time series at one location. To derive information about the spatial turbulent structure some assumptions have to be made. It is common practice to assume the Taylor hypothesis applicable. Firstly we assume that for statistically stationary and horizontal homogeneous conditions time and space averaging may be interchanged. In that case the structure parameter can be derived from a time series of two spatial separated sensors. The next step is to derive the structure parameter from a time series of one sensor alone by applying Taylor hypothesis. This is not strait forward. Since the measurements are taken in a turbulent field the air is advected with variable speed through the sensor. To have a constant separation in space we need a variable separation in time. The consequences of this effect is studied by Lumley (1965) and Wyngaard and Clifford (1977) and applied for spectra, i.e. wavenumber and frequency domain. Here we will follow their lines but now for the space and time domain.

The time domain structure function is defined as:

$$D_{a,t}^2(\Delta t) = \overline{(a(y,t+\Delta t)-a(y,t))^2} \tag{3.5}$$

where overbar denote a time average. Let us assuming that the advection fluctuations are dominated by the large scales L of the turbulence and that the structure of the small scale (x, $U\Delta t$) is independent of the large scale advection fluctuations. Wyngaard and Clifford (1977) state that there is some evidence for this assumption. The time average can be rewritten into an integral over the distribution of all possible wind velocities ($P(u)$) and changed to the spatial formulation of the structure function:

$$D_{a,t}^2(\Delta t) = \int du\ P(u)\ D_a^2((\overline{U}+u)\Delta t) \tag{3.6}$$

where $\overline{U}$ is the main wind vector and $\boldsymbol{u}$ the deviation from the main wind vector. To evaluate the integral a three dimensional Gaussian distribution of the windvector $\boldsymbol{u}$ is assumed with variances deviation σ_u^2, σ_v^2, σ_w^2 and one non-zero covariance, i.e. $\langle uw \rangle$. The structure function is assumed to have a 2/3 power law behaviour. Applying the method of Gaussian averaging described in Chapter 9, we have up to third order:

$$D_{a,t}^2(\Delta t) = D_a^2(\overline{U}\Delta t)\cdot\left(1-\frac{1}{9}\frac{\sigma_u^2}{\overline{U}^2}+\frac{1}{3}\frac{\sigma_v^2}{\overline{U}^2}+\frac{1}{3}\frac{\sigma_w^2}{\overline{U}^2}\right) \tag{3.7}$$

For the current forest site a reasonble approximation is $\sigma_u^2 = 3\ \sigma_w^2$, thus the two corresponding terms in Equation (3.7) cancel. For the forest site the standard deviation of the wind direction for neutral conditions is circa 0.3 rad, this amounts to an overestimation of the space based structure function by the time based structure function of circa 3%. The remaining factor is approximately equal to the $2/3^{th}$ power of the ratio of the average length of the windvector and the length of the average wind vector:

$$D_{a,t}^2(\Delta t) = D_a^2(\overline{U}_{abs}\Delta t) \tag{3.8}$$

Thus by deriving structure parameters from time series we have to apply Taylor-hypothesis with an advection speed equal to the average length of the wind vector. Structure parameters are derived accordingly.

3.4 The influence of increased dissipation variance at smaller scales

In the studies of Kolmogorov (1962) and Obhukov (1962) the influence of intermittency of dissipation is put forward. The variance of dissipation increases when going to increasingly smaller scales. This effect is found to be a function of the ratio between the energy containing scale L and the scale under observation. The consequence is that

$$<\varepsilon^{\beta}> \neq <\varepsilon>^{\beta} \quad for \quad \beta \neq 1 \tag{3.9}$$

This makes the scaling law given in Equation (3.3) ambiguous. Several statistical models are developed, see Kolmogorov (1962), Frisch, Sulem and Nelkin (1978). Anselmet et al. (1984) compared the models with observations. For all models the second order structure function leads to the form

$$D_a^2(x) \sim (\varepsilon x)^{2/3}\left(\frac{L}{x}\right)^{\mu_{2/3}} \tag{3.10}$$

Anselmet et al. find for the exponent $\mu_{2/3}$ a value of -0.05. The consequence is that the structure parameter as defined in Equation (3.4) depends on the lag x even in the inertial subrange and increases with increasing lag. For lag ratios of 2 and 4 the increase is 3.5% and 7% respectively. Translating this to atmospheric sublayer measurements there will be a weak dependence on the measuring height and stability since these are directly related to the dominant length scale. For neutral conditions we have 3.5% increase for a 2 times lower measuring height keeping the lag x equal.

4 Error sources in the measurement of the structure parameter of the vertical wind with a sonic anemometer.

We identify four ways in which the measurements of fine scale wind turbulence are distorted by a sonic anemometer. Here the analysis is performed for the Kaijo-Denki DAT-300 sonic anemometer. Some aspects may differ for other types of sonic anemometers.

a) Filter characteristic of the D/A converter.
b) Line averaging along the transducer path
c) Time delay between upward and downward measurement of the velocity components.
d) Sample and hold of the D/A converter

All this effects are in a sense low-pass filters which affect the sensitivity for small scale turbulence. The method to treat this losses is by transforming to wavenumber domain and calculate spectral transfer functions for each error source. Then with a prescribed turbulence spectrum the total loss can be calculated. An alternative way to estimate the effect of losses is by calculating the effect on the autocorrelation function directly. A disadvantage of that method is that subsequent losses at different places in the measuring system have to be treated simulatiously. An advantage is that it leads directly to expressions in terms of flux or variance loss.

We start from the relation between the structure function and the correlation function. From Equation (3.2) we have:

$$D_a^2(x) = 2\,(R_{aa}(0)-R_{aa}(x)) \tag{4.1}$$

Thus the structure function is the difference between the total variance and the autocorrelation at lag x. The first term contains all spatial scales down to the smallest, whereas the latter contains only scales of the order x and larger. This means that filtering with a characteristic spatial scale of l smaller then x will mainly affect the variance and only slightly the lagged autocorrelation. The effect on the lagged autocorrelation is of the order $(l/x)^2$. The filtered variance is in effect the average over the autocorrelation function over a region of the order l around lag $x = 0$. Using the results of the previous appendix and for l within the inertial subrange we can estimate the loss of variance to be of the order $C_a^2 l^{2/3}$. In formula we have:

$$\tilde{D}_a^2(x) = D_a^2(x)\cdot\left(1+O\left(\frac{l}{x}\right)^2\right)-\beta C_a^2 l^{2/3} \tag{4.2}$$

$$\tilde{C}_a^2(x) = C_a^2(x)\cdot\left(1-\beta\left(\frac{l}{x}\right)^{2/3}+O\left(\frac{l}{x}\right)^2\right) \tag{4.3}$$

β is a constant which depends on the precise filtering that is applied. Equation (4.2) shows that the spectral loss in the structure function is independent of the lag x, provided x is much larger then l. This provides an interesting way to diminish the effect of filtering on the structure function. Let x_1 and x_2 be two lags in the inertial subrange then the difference between the filtered structure functions for these two lags is equal, up to second order, to the difference in the unfiltered structure functions. Thus we have

$$C_a^2 = \frac{\tilde{D}_a^2(x_2)-\tilde{D}_a^2(x_1)}{x_2^{2/3}-x_1^{2/3}}\left(1+O\left(\frac{l}{x}\right)^2\right) \tag{4.4}$$

This opens the possibility of correcting structure parameter measurements for high frequency loss without tedious correction procedures. To proceed we will describe this tedious correction procedure for one of the error sources, i.e. line averaging. We have choosen this example because it also gives results relevant for estimation of high frequency variance losses as will be described in Chapter 5. To calculate the total loss the effects have to be treated simultaneously. This is described in Van der Ploeg (1995), together with the software used to perform the corrections on the data. Figure 4.1 shows the comparison between the two methods for the structure parameter of the vertical wind according to (4.4) and according to Van der Ploeg (1995).

4.1 The effect of line averaging on measured structure parameters of a turbulent windfield.

When measuring wind speeds with a sonic anemometer there will inevitably be some line averaging involved along the transducer path. Here we shall derive the corrections for this effect on the wind structure function under the assumption of homogeneity and local isotropy. In an isotropic turbulent windfield it can be shown (Hinze, 1959) that the correlation wind tensor is given by:

$$\mathbf{R}(\vec{r}) = \{f(r)-g(r)\}\cdot\frac{\vec{r}\times\vec{r}}{r^2}+g(r)\cdot\mathbf{I} \tag{4.5}$$

$\mathbf{I}$ is the unit tensor $\vec{r}$ is the seperation in space. This form is the most general second rank tensor which can be build from $\vec{r}$ alone. The functions f and g are related through the continuity equation. $f(r)$ describes the correlation function for the wind component along $\vec{r}$, whereas $g(r)$ describes the correlation for a wind component perpendicular to $\vec{r}$. For the inertial subrange it can be shown that the functions $f(r)$ and $g(r)$ are:

$$\begin{aligned} f(r) &= f(0)-\frac{3}{8}C_{\perp}^2 r^{2/3} \\ g(r) &= g(0)-\frac{4}{8}C_{\perp}^2 r^{2/3} \end{aligned} \tag{4.6}$$

where the index $\perp$ indicates the component perpendicular to the separation vector $\vec{r}$. We observe the well known 4/3 ratio between correlation loss as a function of distance for the lateral and longitudinal components. $f(0)$ and $g(0)$ are related to the variances of the fluctuations. The variances are dominated by the large scale fluctuations of the turbulence. For wall bounded shear flows the turbulence is not isotropic on the large scale and thus this terms do not fitt into the isotropic framework. For our purpose, the analysis of the structure functions, we are only interested in deviations from this variance and thus in the end the large scale contributions cancel.

Assumed is that the structure functions are measured in the time domain and transformed with Taylor hypothesis to the spatial domain along the direction of the main wind speed vector given by the unit vector $\vec{e}_U$. One transducer pair of a sonic anemometer defines a direction $\vec{\mathbf{e}}_A$ along which the wind is measured. In principle the transducer A then measures the average over the transducer path of $U_A = \vec{U}\cdot\vec{e}_A$. The geometry of the problem is cylindrical symmetric with cos(θ), the cosine between the two directions as a parameter. For U_A we derive from Equation (4.5) with the identity:

$$\vec{e}_A\cdot\frac{\vec{r}\times\vec{r}}{r^2}\cdot\vec{e}_A = \cos^2\theta \tag{4.7}$$

$$R_{AA}(r,\theta) = R_{AA}(0)-\frac{1}{2}C_{\perp}^2 r^{2/3}\left(1-\frac{1}{4}\cos^2\theta\right) \tag{4.8}$$

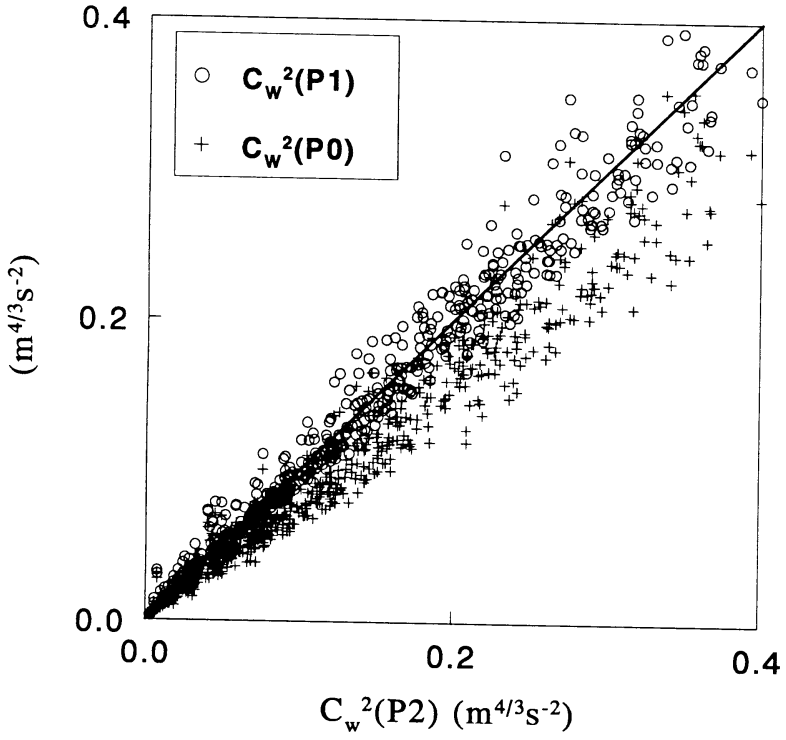

Figure 4.1 Comparison of two correction procedures for structure parameter of the vertical wind. P1 and P2 refer to two correction procedures and P0 refer to uncorrected values (see text).

and we find

$$C_A^2 = C_\perp^2 \cdot (1 - \frac{1}{4}\cos^2\theta) \tag{4.9}$$

The result of a measurement along the transducer path can be written as:

$$\tilde{U}_A(\vec{r}) = \int_{-l/2}^{l/2} U_A(\vec{r}+s\vec{e}_A)ds \tag{4.10}$$

Since the structure functions are measured, with the Taylor hypothesis, as seperations x along the mean wind directions we write down the particular autocorrelation function:

$$\begin{aligned}\tilde{R}_{AA}(x\vec{e}_U) &= \frac{1}{l^2}\int_{-l/2}^{l/2}\int_{-l/2}^{l/2} ds ds' \; \vec{e}_A \cdot \mathbf{R}([s-s']\vec{e}_A + x\vec{e}_U)\cdot\vec{e}_A \\ &= \int_{-1}^{1} d\eta \; (1-|\eta|) \; \vec{e}_A \cdot \mathbf{R}(\eta l\vec{e}_A + x\vec{e}_U)\cdot\vec{e}_A\end{aligned} \tag{4.11}$$

Substituting Equation (4.5) and using the identities

$$
\begin{aligned}
\vec{y} &= \eta l\vec{e}_A + x\vec{e}_U \\
(\vec{y}\cdot\vec{e}_A)^2 &= y^2 - x^2\sin^2(\theta) \\
y^2 &= \left[(\eta p)^2 + 2\eta p\cos(\theta) + 1\right]\cdot x^2
\end{aligned}
\tag{4.12}
$$

where $p = l/x$, we arrive at:

$$
\begin{aligned}
\tilde{R}_{AA}(x\vec{e}_U) &= R_{AA}(0) - \frac{1}{2}\frac{C_A^2 x^{2/3}}{1 - {}^1/_4\cos^2\theta} I(p,\cos\theta) \\
I(p,\cos\theta) &= \int_{-1}^{1} d\eta(1-|\eta|)\frac{{}^3/_4\left[(\eta p)^2 + 2\eta p\cos\theta + 1\right] + {}^1/_4\sin^2\theta}{\left[(\eta p)^2 + 2\eta p\cos\theta + 1\right]^{2/3}}
\end{aligned}
\tag{4.13}
$$

First we shall examine the limiting behaviour of the integral.

The loss of variance due to the line averaging is obtained by letting x go to zero, or equivalently p grow without limit:

$$
\lim_{p\to\infty} I(p,\cos\theta) = \frac{27}{80}p^{2/3} \tag{4.14}
$$

which results in:

$$
\tilde{R}_{AA}(0) = R_{AA}(0) - \frac{1}{2}\cdot\frac{27}{80}\frac{C_A^2 l^{2/3}}{1 - {}^1/_4\cos^2\theta} \tag{4.15}
$$

With Equation (4.9) we observe that the variance loss is independent of direction.

The limit for large separations i.e. p small is after straight forward approximation:

$$
\tilde{R}_{AA}(x\vec{e}_U) = R_{AA}(0) - \frac{1}{2}C_A^2 x^{2/3}\left(1 + p^2\,\frac{\left(\frac{1}{72} + \frac{7}{108}\cos^2\theta - \frac{5}{54}\cos^4\theta\right)}{1 - \frac{1}{4}\cos^2\theta}\right) \tag{4.16}
$$

For transducers parallel and perpendicular to the main wind respectively we find:

$$
\begin{aligned}
\tilde{R}_{\perp\perp}(x\vec{e}_U) &= R_{\perp\perp}(0) - \frac{1}{2}C_\perp^2 x^{2/3}\left(1 + \frac{1}{72}p^2\right) \\
\tilde{R}_{\parallel\parallel}(x\vec{e}_U) &= R_{\parallel\parallel}(0) - \frac{1}{2}C_\parallel^2 x^{2/3}\left(1 - \frac{1}{54}p^2\right)
\end{aligned}
\tag{4.17}
$$

the coefficients of the second order terms suggest that this approximations are accurate down to rather small values. For one special case we can test this suggestion. For the parallel case ($\theta = 0$) we can test this suggestion rigorously ecause an exact solution to the integral in Equation (4.13) can be found:

$$
I(p,\cos(\theta=0)) = \frac{3}{4}\int_{-1}^{1} d\eta\cdot(1-|\eta|)\sqrt[3]{(1+\eta p)^2} \tag{4.18}
$$

For $p < 1$, i.e. $l <$ **x**, we find after some transformation of variables

$$
I(p,1) = \frac{3}{4}\cdot\frac{1}{p^2}\left(\frac{9}{40}\left[(1+p)^{8/3} + (1-p)^{8/3} - 2\right]\right) \qquad 0<p<1 \tag{4.19}
$$

For $p = 1$ the exact solution give 0.021 for the correction term, whereas the second order approximation give 0.019. Thus indeed the second order effect remains small for p up to 1.

For the structure function we find:

$$\tilde{D}_a(x) = D_a(x) - \frac{1}{2}\cdot\frac{27}{80}\frac{C_A^2 l^{2/3}}{1-{}^1/_4\cos^2\theta} \tag{4.20}$$

This form confirms the reasoning that lead us to the simple correction method described in Equation (4.4)

5 High frequency loss in flux estimates due to line averaging.

5.1 Introduction

In the literature several studies can be found on the spectral loss due to line averaging and sensor seperation. Almost all these studies are concerned with the loss in variance of scalars and velocities. The reason is that for these quantities the three dimensional structure function or if you like the three dimensional wavenumber spectrum in the inertial subrange can adequately be described with the assumption of isotropy. This assumption greatly simplifies the form of the spectrum. This exercise has been done by Kaimal et al. (1968) for the wind components and for scalars by Andreas (1981) and Kohsiek (1984).

Moore (1986) suggests that the loss in for example the temperature flux <wt> can be described in spectral terms by the product of the square root of the transfer functions for σ_w^2 and σ_t^2 transfer function. As shown by Kristensen and Fitzjarrald (1984), hereafter called KF84, this can not be correct. The reason is that the transfer functions depends on the three dimensional spectrum of the quantities under consideration and this spectrum is not known for fluxes. This is because a flux spectrum can not be isotropic and in practice we have only access to the one dimensional spectrum in the mean wind direction. To make progres KF84 tries to find a simple non-isotropic vectorial spectrum. They start with the assumption of rotation symmetry around the vertical axis, allowing for a vertical flux. Consequently the horizontal fluxes are zero due to mirror-symmetry. This is justified somewhat by observations since the cross-spectrum of <*ut*> tends to fall off more quickly then do <*wt*> (Kaimal et al., 1972). Together with the condition of divergence free flow they arrive at an expression for the three dimensional spatial cross spectrum for *w* and *s*, where now *s* is an arbitrarily scalar quantity:

$$\phi_{3S}(\vec{k}) = A(k,k_3)\left(1-\frac{k_3^2}{k^2}\right) \tag{5.1}$$

Although the form has already been greatly restricted it is still not tractible due to the dependence of A on two variables. They then assume that A is only dependent on k. In the inertial subrange A falls of with a 7/3 + 2 power of k.

Here we try to analyse the problem of line averaging in terms of spatial correlation. First we derive an expression for a path in the direction of the mean wind. This is the situation where we have information from time series of point measurements. Then we use the spectral vector model of KF84 to assess the difference when the path is perpendicular to the mean stream, typical for flux measurements. The present analysis is typical for a temperature flux measured with a sonic anemometer where w and s are measured along the same transducer path.

5.2 Relation between Co-spectrum and structure function

We the co-spectral form defined by KF84 based on Kaimal (1972) for the inertial subrange:

$$Co(k) = \beta z\langle ws\rangle(|k|z)^{-7/3} \quad , kz \gg 1 \tag{5.2}$$

where β is a stability dependent parameter. For the flux we have

$$\langle ws \rangle = \int_0^\infty Co(k)\, dk \tag{5.3}$$

The spectrum is related to the along wind direction thus we can relate the spectrum to the structure function with lags in the along wind direction:

$$D_{ws}(x\vec{e}_u) = 2\{R_{ws}(0) - R_{ws}(x\vec{e}_u)\} = 2\int_0^\infty Co_{ws}(k)\cdot(1-\cos(kx))dk \tag{5.4}$$

By substituting the inertial sub range form for the co-spectrum and realising that for $x << z$ the precise form for small wavenumbers become unimportant for the evaluation of the integral we have:

$$D_{ws}(x\vec{e}_u) = 2\beta\langle ws \rangle \left(\frac{x}{z}\right)^{4/3} \int_0^\infty y^{-7/3}(1-\cos(y))dy \qquad ,x \ll z \tag{5.5}$$

Numerical integration of the integral gives 1.523.

5.3 Loss of covariance due to line averaging in terms of the structure function

Analogous to the derivation in appendix 4 we can obtain an expression for the flux loss:

$$\delta\langle ws \rangle = \int_0^\infty (1-\eta) D_{ws}(\eta l\vec{e}_u)d\eta \tag{5.6}$$

Substituting Equation (5.5) results in:

$$\delta\langle ws \rangle = 2\cdot 1.523\cdot\frac{9}{70}\beta\left(\frac{l}{z}\right)^{4/3}\langle ws \rangle \tag{5.7}$$

We now have to find the magnitude of β. This can be derived from the co-spectrum given by Kaimal et al. (1972) in the frequency domain (n):

$$C_{ws}(n) = \frac{1.62}{(2\pi)^{4/3}}\langle ws \rangle\, H(z/L)\, f^{-4/3}\, n^{-1} \tag{5.8}$$

with $H(z/L) = 1$ for unstable cases and $H(z/L) = 1+6.4\ z/L$ for stable cases. f is the dimensionless frequency nz/U. Converting to wavenumber domain with $dk = 2\rho/U \bullet dn$ we find $\beta = 1.62\ H(z/L)$. Thus finally we have for the flux loss due to line averaging along a path parallel to the main wind:

$$\delta\langle ws \rangle = 0.65\cdot H(z/L)\left(\frac{l}{z}\right)^{4/3}\langle ws \rangle \tag{5.9}$$

In the same way an expression for the stress $\langle uw \rangle$ can be derived:

$$\delta\langle uw \rangle = 0.22\cdot G(z/L)\left(\frac{l}{z}\right)^{4/3}\langle uw \rangle \tag{5.10}$$

where $G(z/L) = 1$ for unstable cases and $G(z/L) = 1+7.9\ z/L$ for stable cases.

5.4 Loss for a path perpendicular to the main wind

The previous analysis is based on the one-dimensional spectrum and the structure function in the along wind direction. To get expressions for a path perpendicular to the main wind we need the

one dimensional co-spectrum for <*ws*> or the corresponding structure function in the vertical direction. The full correlation vector is related to the full three dimensional spectrum through:

$$R_{iS}(\vec{r}) = \iiint \phi_{iS}(\vec{k}) e^{-i\vec{k}\cdot\vec{r}}\, d^3\vec{k} \tag{5.11}$$

where i denote one of the velocity components u,v or w.

For the along wind direction we have the relation between the correlation function for <*ws*> and the corresponding one dimensional spectrum F^1_{3S} which is in fact 1/2 Co_{ws} from the previous paragraph:

$$\begin{aligned} R_{3S}(x\vec{e}_1) &= \int dk_1 e^{-ik_1 x} \iint dk_2 dk_3 \phi_{3S}(\vec{k}) \\ &= \int dk_1 e^{-ik_1 x} F^1_{3S}(k_1) \end{aligned} \tag{5.12}$$

For the direction perpendicular to the wind we have the relation between the correlation function for <*ws*> and the corresponding one dimensional spectrum F^3_{3S}:

$$\begin{aligned} R_{3S}(z\vec{e}_3) &= \int dk_3 e^{-ik_3 z} \iint dk_1 dk_2 \phi_{3S}(\vec{k}) \\ &= \int dk_3 e^{-ik_3 z} F^3_{3S}(k_3) \end{aligned} \tag{5.13}$$

To evaluate the one-dimensional spectra we use the axisymmetric spectral model of KF84 for the inertial subrange:

$$\begin{aligned} \phi_{3S}(\vec{k}) &= A(k)\left(1 - \frac{k_3^2}{k^2}\right) \\ A(k) &= \gamma \frac{k^{-p}}{k^2} \end{aligned} \tag{5.14}$$

After some algebra we find:

$$\begin{aligned} F^1_{3S}(k) &= \gamma \cdot \pi \frac{2(p+1)}{p(p+2)}\, k^{-p} \\ F^3_{3S}(k) &= \gamma \cdot \pi \frac{4}{p(p+2)}\, k^{-p} \end{aligned} \tag{5.15}$$

Using p = 7/3, the flux spectrum value, we find that the vertical spectral correlation is 3/5th of the along wind spectral correlation. The same will hold for the corresponding structure functions in the inertial subrange:

$$D_{3S}(y\vec{e}_3) = \frac{3}{5} D_{3S}(y\vec{e}_1) \tag{5.16}$$

5.5 Results

For the current location we can now estimate flux losses due to line averaging. We take l = 0.2 m and z = 18 m above the displacement height. For neutral conditions a loss of 0.1 % is found, for stable conditions at z/L = 1 we find 0.7 % and for z/L = 2 we have 1.2 %. Thus in all cases the loss is negligible. For the stress we cannot give definite values. To derive results for <*uw*> an axisymmetric spectral tensor have to be found. This is not attempted here. From the previous paragraph we find that for the along wind case loss in the stress is a factor 3 smaller than for the scalar flux. Thus it seems save to assume that fractional losses in <*uw*> will be smaller than for the scalar flux and therefor be also negligible.

6 Low frequency loss in fluxes due to a finite averaging time.

6.1 Introduction

Turbulent transport in the turbulent surface layer takes place over a wide range of frequencies. Especially variances of horizontal wind and scalars in the surface layer during convective conditions have large contributions in the low frequency range. For the vertical wind speed this contributions are much smaller because the vertical wind speed is constraint by the surface. The extension of co-spectra of scalars or horizontal wind and vertical wind at the low-frequency end are somewhere between this two extremes. Kaimal et al (1972) give surface layer spectra and co-spectra for various stabilities.

In micro-meteorogy it is common practice to determine eddy-correlation surface fluxes on a time scale of an hour and perform some kind of detrending on the data. This can be a linear detrending or by taking a shorter averaging time and subsequently averaging over a series of these fluxes. The time scale of an hour is a compromise to reach a statistical stable estimate of the flux (see Lumley and Panofsky, 1964) on the one hand and the need to have approximately stationary conditions on the other hand. By detrending the problem of stationarity is somewhat relaxed. But in practice one is not sure that the trend is part of low frequency contributions to the turbulent flux.

Here we are interested in the loss of the low-frequency contribution to the flux due to finite averaging times. This will be determind on the basis of the spectra presented by Kaimal et al. (1972). In recent years there has been speculation about meso-scale contributions to the vertical flux due to terrain contrasts or circulation patterns relate to cloud streets. This topic is far from being solved and will not be treated here

6.2 Low frequency spectral loss

Let $w(t)$ and $c(t)$ be stationary turbulent time series of the vertical wind speed and a scalar quantity respectively, both with zero mean. Let us denote by $< >_T$ an average over a period T and by $\{ \}$ an average over an ensemble of $< >_T$ averages. A turbulent flux over the period T without detrending is then determined according to:

$$F_C^T = \frac{1}{T}\int_{-T/2}^{+T/2} (w-\langle w\rangle_T)\cdot(c-\langle c\rangle_T)dt \tag{6.1}$$

Writing out the product and perform an ensemble average we arrive at:

$$\{F_C^T\} = F_C - \frac{1}{T^2}\int_{-T/2}^{+T/2} dt \int_{-T/2}^{+T/2} dt' \ \{w(t)\cdot c(t')\} \tag{6.2}$$

where F_C is the actual flux. The second term on the right hand side represents the spectral loss due to a finite averaging time. Equation (6.2) can be written in terms of the time correlation function $R_{wc}(\tau)$, which due to the stationarity of the time series depends only on the time difference τ = t-t'.

$$\{F_C^T\} = F_C\left(1-\frac{1}{T}\cdot\int_{-T}^{+T} d\tau\ (1-\frac{|\tau|}{T})\ R_{wc}(\tau)\right) \tag{6.3}$$

In the surface layer it is found that R is symmetric and the integral timescale is defined as:

$$J_{wc} = \frac{1}{R_{wc}(0)} \int_{-\infty}^{+\infty} R_{wc}(\tau)\, d\tau \tag{6.4}$$

If $T >> J_{wc}$ we have:

$$\{F_C^T\} = F_C \left(1 - \frac{J_{wc}}{T}\right) \tag{6.5}$$

The integral timescale is related to the spatial integral scale through the wind speed according to $L_{wc} = J_{wc}U$. The integral length scale in the surface layer is a function of height z and stability ζ. By introducing the dimensionless integral length scale $l_{wc}(\zeta) = L_{wc}/z$, we arrive at:

$$\{F_C^T\} = F_C \left(1 - l_{wc}(\zeta) \cdot \frac{z}{UT}\right) \tag{6.6}$$

In the literature cross-spectra are given rather then correlation functions. Thus to proceed we rewrite the loss term in terms of frequencies. The cross spectrum and correlation function are related by:

$$\begin{aligned} R_{wc}(\tau) &= \int_{-\infty}^{+\infty} S_{wc}^f(f) e^{-2\pi i f \tau}\, df \\ S_{wc}^f(f) &= \int_{-\infty}^{+\infty} R_{wc}(\tau) e^{+2\pi i f \tau} d\tau \end{aligned} \tag{6.7}$$

From this we derive that $S_{wc}^f(0) = J_{wc}$. By substituting Equation (6.7) into Equation (6.3) and perform the time integration we arrive at a spectral representation of the loss:

$$Loss = \int_{-\infty}^{+\infty} S_{wc}^f(f) \cdot \frac{\sin^2(\pi f T)}{(\pi f T)^2} df \approx 2 \cdot \int_0^{+2/T} S_{wc}^f(f) \cdot \left(1 - \frac{fT}{2}\right) df \tag{6.8}$$

It is observed that a low pass filter is applied to the spectrum. The filter is represented graphically in Figure 6.1. Also an triangular approximation to the filter is represented with which further integration can be performed.

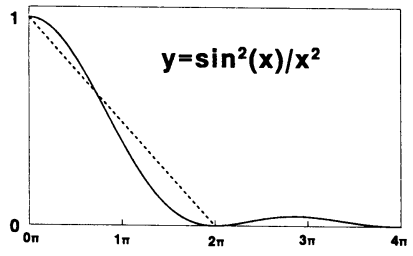

Figure 6.1 High pass filter together with its triangular approximation.

To proceed we use the surface layer spectra given by Kaimal et al. (1972). The general form of the cross-spectrum in terms of the dimensionless frequency $n = fz/U$ is:

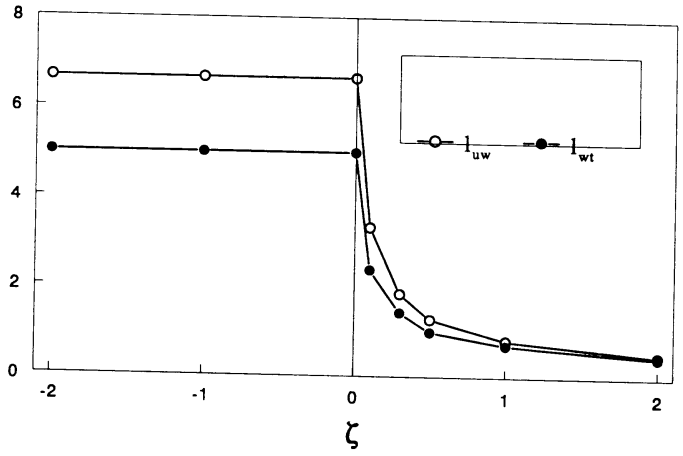

Figure 6.2 Dimensionless integral length scale as function of stability for stress and for heat flux (based on Kaimal,1972).

$$\frac{U}{z}S_{wc}^{f}(f) = S_{wc}^{n}(n) = \frac{1}{2}F_C\frac{a}{\left(1+n\cdot\frac{a}{p-1}\right)^{p}} \tag{6.9}$$

Here the formulation is modified to be in line with the normalisation over the entire frequency domain instead of the half infinite domain used by Kaimal. It follows that $S^{n}_{wc}(0) = l_{wc}F_C$ and thus $a = 2l_{wc}$.

It can be shown that the maximum of the function $nS^{n}_{wc}(n)$ is at $n = 1/(2l_{wc})$. This makes it possible to estimate l_{wc} for different stabilities from the graphical representation of the spectra given by Kaimal. Figure 6.2 shows the results of this estimation. The two curves are conveniently parameterised as:

$$\begin{aligned} l_{uw}(\zeta) &= \frac{J_{uw}U}{z} = \frac{L_{uw}}{z} = \frac{6.7}{1+6.7\zeta} \\ l_{wt}(\zeta) &= \frac{J_{wt}U}{z} = \frac{L_{wt}}{z} = \frac{5.0}{1+6.7\zeta} \end{aligned} \tag{6.10}$$

We are now in a position to evaluate the loss integral:

$$\begin{aligned} Loss &= 2\chi F_c\int_0^1 dy\left(1+y\frac{2\chi}{p-1}\right)^{-p}(1-y) \\ y &= fT\ , \quad \chi = \frac{l_{wc}z}{UT} \end{aligned} \tag{6.11}$$

Resulting in:

$$Loss = F_c\cdot\left(1+\frac{1}{2\chi}\frac{p-1}{p-2}\cdot\left((1+\frac{p-1}{2\chi})^{2-p}-1\right)\right) \tag{6.12}$$

This complicated looking expression approaches χF_C for χ going to 0, in concord with the limiting

case given in Equation (6.6). Figure 6.3 shows the fractional loss as a function of χ for the flux spectrum case, $p = 7/3$.

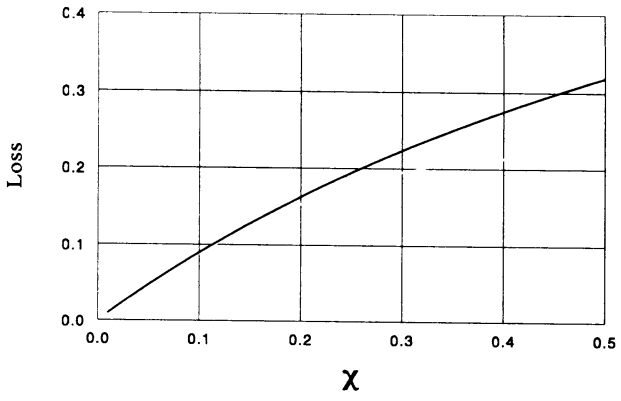

Figure 6.3 Low frequency spectral loss as function of $\chi = l_{wc}(\zeta)z/(UT)$.

From the limiting case we see that for u_* the absolute loss is approximately independent of wind speed:

$$u_*(uncor) = u_* - \frac{l_{uw} z}{2T} \frac{u_*}{U} \tag{6.13}$$

6.3 Results

For the current location we have z=18m above the displacement height, $z_0 = 2$ m and $T = 600$ s. For neutral conditions we have for the momentum flux $\chi = 0.20/U$, which results in a loss of 16% at $U = 1$ m s^{-1} and a loss of 6% at $U = 3$ m s^{-1}. In absolute sense we have an underestimation of u_* by 0.018 m s^{-1}. Losses in calar fluxes are 80% of the stress losses.

7 Corrections for zero-crossing jump in the sonic anemometer windspeed

A close inspection of the recalibration results of the sonic anemometer after the experiment revealed a subtle error in the D/A converter of the sonic anemometer electronics causing a jump of 0.14 m s^{-1} in the wind signals when crossing sign. To be precise the windspeed is correct for positive values and 0.14 m s^{-1} to low for negative values. Here the consequences are derived for covariances involving the vertical wind velocity and for the structure parameters of the vertical wind.

7.1 Corrections for covariances with the vertical wind

Let us quit generally assume that the measured vertical windspeed ($\tilde{W}$) and the true vertical windspeed (W) are related by:

$$\tilde{W}=W+F(W) \tag{7.1}$$

To investigate the influence of the deviation $F(W)$ on the variance of W and the covariance of W with some other turbulent quantity C we split the quantities in mean and fluctuating parts:

$$\begin{aligned} W&=<W>+w \\ \tilde{W}&=<\tilde{W}>+\tilde{w} \\ C&=<C>+c \end{aligned} \tag{7.2}$$

where the brackets denote some sort of averaging, in our case averaging over time. The variance of $\tilde{W}$ and W are then related by:

$$<\tilde{w}\tilde{w}>=<ww>+2<wF(W)>+<\{F(W)-<F(W)>\}^2> \tag{7.3}$$

The covariance between C and $\tilde{W}$ and W respectively are related by:

$$<\tilde{w}c>=<wc>+<F(W)c> \tag{7.4}$$

In the following it will be understood that $f(w) = F(<W>+w) = F(W)$.
Let $p(w,c)$ be the joint probability distribution of w and c, then the second term on the r.h.s of equation (7.4) can be written as:

$$<f(w)c>=\int_{-\infty}^{\infty}\int_{-\infty}^{\infty} f(w)c\cdot p(w,c)\cdot dw\cdot dc \tag{7.5}$$

To proceed we assume that the two turbulent quantities w and c follow a joint bi-Gaussian distribution (see Panofsky and Dutton, 1984):

$$p(w,c)=\frac{1}{2\pi\sigma_w\sigma_c\sqrt{1-R^2}}\ Exp\left(-\frac{(\frac{w}{\sigma_w})^2+(\frac{c}{\sigma_c})^2-2R\frac{wc}{\sigma_w\sigma_c}}{2(1-R^2)}\right) \tag{7.6}$$

where R is the correlation coefficient between w and c.
Substituting this in equation (7.5) and scaling variables according to:

$$\begin{aligned} w&=\omega\cdot\sigma_w \\ c&=\gamma\cdot\sigma_c \\ f(w)&=\Delta w\cdot g(\omega) \end{aligned} \tag{7.7}$$

where Δw is a characteristic velocity scale for the deviation in w, gives:

$$\langle f(w)c\rangle = \frac{\sigma_c \Delta w}{2\pi\sqrt{1-R^2}} \int_{-\infty}^{\infty} d\omega \cdot g(\omega) \int_{-\infty}^{\infty} d\gamma\gamma \cdot Exp\left(-\frac{\omega^2+\gamma^2-2R\omega\gamma}{2(1-R^2)}\right) \tag{7.8}$$

The coordinate translation $\gamma \rightarrow \gamma + R\omega$ creates a perfect square of γ in the exponent of equation (7.8):

$$\langle f(w)c\rangle = \frac{\sigma_c \Delta w}{2\pi\sqrt{1-R^2}} \int_{-\infty}^{\infty} d\omega \cdot e^{-\frac{1}{2}\omega^2} g(\omega) \int_{-\infty}^{\infty} d\gamma \cdot (\gamma + R\omega)\ Exp\left(-\frac{\gamma^2}{2(1-R^2)}\right) \tag{7.9}$$

after which the integral over γ can be performed. Note that the uneven component in the last integral over γ sums to zero. With the identity:

$$\int_{-\infty}^{\infty} e^{-\frac{1}{2}x^2} dx = \sqrt{2\pi} \tag{7.10}$$

we find then:

$$\langle f(w)c\rangle = \frac{R\sigma_c \Delta w}{\sqrt{2\pi}} \int_{-\infty}^{\infty} d\omega \cdot e^{-\frac{1}{2}\omega^2} g(\omega)\omega \tag{7.11}$$

Noting that $R\sigma_w\sigma_c = \langle wc\rangle$ by definition we can rewrite this into:

$$\langle f(w)c\rangle = \langle wc\rangle \frac{\Delta w}{\sigma_w} \cdot \frac{1}{\sqrt{2\pi}} \int_{-\infty}^{\infty} d\omega \cdot e^{-\frac{1}{2}\omega^2} g(\omega)\omega \tag{7.12}$$

The integral is normalised which assures that it will be of the order 1. We can test equation (7.12) by substituting $g(\omega) = \omega$ and $\Delta w = \sigma_w$, we then find $\langle f(w).c\rangle = \langle wc\rangle$ which is true in this case. It is observed that only the anti-symmetric part of $g(\omega)$ contributes to the integral. Dependent on the form of $g(\omega)$ it can be advantageous to split the integral in a positive and negative part and then substitute $y = \frac{1}{2}\omega^2$:

$$\langle f(w)c\rangle = \langle wc\rangle \frac{\Delta w}{\sigma_w} \cdot \frac{1}{\sqrt{2\pi}} \int_{0}^{\infty} dy \cdot e^{-y} \left(g(+\sqrt{2y}) - g(-\sqrt{2y})\right) \tag{7.13}$$

For the case of a jump at $w = 0$ we find:

$$\langle f(w)c\rangle = 0.40\langle wc\rangle \frac{\Delta w}{\sigma_w} \tag{7.14}$$

In practice $\langle W\rangle$ is not equal to zero due to offsets in the electronics and due to flow obstruction around the sonic probe or misalignment of the sonic probe. If $\langle W\rangle$ is not zero we have a jump at $w = -\langle W\rangle$. This will decrease the $\langle f(w).c\rangle$, however in practice $\langle W\rangle$ is much smaller then σ_w and therefor we can neglect this effect and assume that the jump occur at $w = 0$.

7.2 Corrections for the structure parameter of the vertical wind

The structure parameter of the vertical wind is derived by taking at regular time intervals τ two samples separated by a short time interval Δt. From such a series of N samples the structure function is derived:

$$D_w^2(\Delta\tau)=\frac{1}{N}\sum_{n=1}^{N}\left[w(n\tau+\Delta t)-w(n\tau)\right]^2 \tag{7.15}$$

If the number of zero-crossing between two samples from which the difference are taken is odd, an artificial contribution is added to the sum of equation (7.15). Let us denote the chance that an odd number of zero crossings occur between to samples with lag Δt by $P_0(\Delta t)$. We can discriminate up going and down going crossings. In both cases the artificial jump acts to increase the difference between the subsequent samples. The contribution to the sum in equation (7.15) for both these cases then is:

$$\left[w(t+\Delta\tau)-w(t)\right]^2+2\Delta w\cdot\left|w(t+\tau)-w(t)\right|+(\Delta w)^2 \tag{7.16}$$

This leads to the expression for the distorted structure function:

$$\tilde{D}_w^2(\Delta t) = D_w^2(\Delta t) + P_Z(\Delta t)\left(2\Delta w<\left|w(t+\Delta t)-w(t)\right|>+(\Delta w)^2\right) \tag{7.17}$$

It is now the task to derive an expression for $P_0(\Delta t)$ in terms of measured quantities.

7.3 Parametrisation of the frequency of zero-crossing

Here we shall analyse the problem in terms of the more fundamental spatial point of view. We define the number of zero-crossings per unit length of the vertical wind $w(x)$ by $N_0(0)$. Let η be the Kolmogorov length scale. We can assume that the smallest separations between subsequent zero-crossings are of the order of η. The chance $P_0(x)$ that an odd number of zero-crossings occurs between two samples of w separated by $x << \eta$ is $xN_0(0)$. For separations much larger then the integral length scale L, $P_0(x) = 0.5$. It is convenient to define $N_0(x)$ as the chance that an odd number of zero crossings occur between two samples at lag x divided by the lag. For small values of x, $N_0(x)$ approaches $N_0(0)$. For large values of x, $N_0(x)$ goes to zero inversely proportional to x.

The problem of zero-crossings in a turbulent signal is closely related to the theory of extreme values. In general terms it is the chance of exceeding a certain threshold value for a stochastic signal with a given autocorrelation function. Rice (1945) shows that the number of zero crossings is related to the variance of the first derivative of the signal and the variance of the signal itself. It can be shown that the total number of zero crossings per unit length is related to the Taylor microscale:

$$N_0(0) = \frac{1}{\pi}\frac{\sigma_{\partial w/\partial x}}{\sigma_w} = \frac{\sqrt{2}}{\pi}\frac{1}{\lambda} \tag{7.18}$$

He also notes that the distribution of lengths between subsequent zero-crossings is a more difficult problem and lacks a general solution. This distribution determines the behaviour of the function $N_0(x)$. Obviously this is related to the behaviour of the spectrum at all different scales. In our case we are interested in the behaviour of $N_0(x)$ in the inertial subrange. We may hope to derive a scaling law for this range since only a limited number of parameters define the structure of the inertial subrange.

Let us argue as follows. The energy containing eddies have a length scale of z and a velocity scale of σ_w. At length scales one octave smaller there are two times more eddies. This increase in number and decrease in size continues through the inertial subrange down to the viscous scale. This is the concept of the energy cascade. The large eddies advect the smaller eddies. The large scale eddies has zero crossings. In regions of these eddies where the vertical velocity is large, smaller eddies are not capable of inducing zero crossings. In regions where the vertical velocity approaches zero smaller and smaller eddies are capable of inducing zero-crossings.

Close to a large eddy induced zero-crossing we have a velocity field due to this large eddy that deviate from zero linearly with the distance y from the zero-crossing:

$$w_L(y) \sim \frac{y}{z}\sigma_w \tag{7.19}$$

Eddies of scale x in the inertial subrange have a characteristic velocity scale given by the square root of the structure function

$$v(x) = D_w(x) = C_w\, x^{1/3} \tag{7.20}$$

By equating the velocities $w_L(y)$ and $v(x)$, a region y is found were eddies of size x are capable of inducing zero-crossings. The number of eddies of scale x in this region is y/x, and with the observation that this give the number of zero-crossings over a distance of order z we have for the number of zero-crossing density induced by eddy size x, denoted by a small letter n:

$$n_0(x) \sim \frac{C_w}{\sigma_w}\, x^{-2/3} \tag{7.21}$$

Eddies much smaller then x will in general contribute an even number of zero-crossings. On the other hand summing Equation (7.21) over the octaves larger then x doesn't affect the scaling law, it only gives a larger constant of proportionality. Thus we have the scaling law.

$$N_0(x) = \beta \frac{C_w}{\sigma_w}\, x^{-2/3} \tag{7.22}$$

where the constant β is introduced. It can be shown that the inertial subrange expression for $N_0(x)$ approaches $N_0(0)$ for x several times η the Kolmogorov length scale. This is consistent with the idea that zero-crossings can be induced by scales down to the kolmogorov scale. For the chance of having an odd number off zero crossings we have:

$$P_0(x) = \beta \frac{C_w}{\sigma_w}\, x^{1/3} = \beta \frac{D_w(x)}{\sigma_w} \tag{7.23}$$

On the basis of 15 days of 5 Hz sampling in november 1993, the zero crossing frequency over half hour intervals were determined for six different time intervals τ ranging from 0.2 to 1.2 s. With Taylor hypothesis the frequencies were transformed in wavenumbers. Figure 7.1 shows $N_0(x)$ scaled on C_w and σ_w as function of lag x, together with the $-2/3_{rd}$ power law with a constant of proportionality $\beta = 0.3$. It is observed that the measurements follow the scaling law over a remarkably large range considering the measuring height of 18 m above the displacement height. Only for lags smaller then 0.8 m deviations occur. This shows the influence of limited response of the sonic anemometer which has a path length of 0.2m.

The relation between the average absolute difference between subsequent w-samples and the structure function was investigated on the basis of the same sample registration. If the difference were Gaussian distributed we would have $< | w(t+\tau)-w(t) | > = 0.798 \cdot D_w$. A slightly different factor of 0.72 was found, indicating that the distribution of $w(t+\tau)-w(t)$ has more pronounced tails as can be expected in intermittent flow. If this observation is used in equation (7.17) together with equation (7.23), we end up with:

$$\tilde{D}_w^2(\tau) = D_w^2(\tau)\left(1 + 1.44\beta \frac{\Delta w}{\sigma_w}\right) + \beta \frac{D_w(\tau)}{\sigma_w}(\Delta w)^2 \tag{7.24}$$

It is observed that the correction of the structure function is independent of the sample time. For

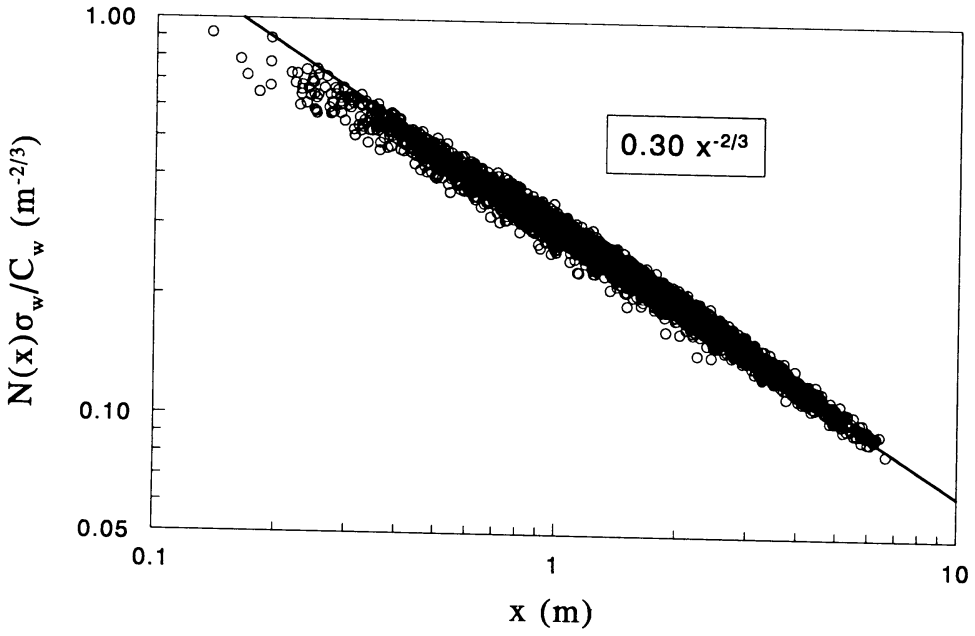

Figure 7.1 Dimensionless zero-crossing chance density as function of lag

the structure parameter we find:

$$\tilde{C}_w^2(\tau)=C_w^2(\tau)\ (1+1.44\beta\frac{\Delta w}{\sigma_w})+\beta\ \frac{C_w(\tau)}{\sigma_w\ (U\tau)^{1/3}}\ (\Delta w)^2 \qquad (7.25)$$

Corrections are performed on the data by solving Equation (7.25).

8 Angle dependence of the Sonic Windspeed

8.1 Introduction

The problem of flow distortion induced errors in sonic anemometer measurements has received a lot of attention in the literature. The windvector at the measuring paths of the sonic anemometer deviate from the free stream wind vector because of transducer shadowing, flow distortion by the supporting frame and the flow obstruction of the boom the sonic probe is mounted on. Kaimal (1979), Hanafusa et al. (1982) and Wyngaard and Zhang (1985) discuss the transducer shadow effect for several sonic anemometers. The lather conclude that the Kaijo Denki improved transducer shape gives deviations in the response only for angles of onflow smaller then 30°. Here we concentrate on the KAIJO DENKI (DAT-300) probe configuration, which has this improved transducer shape and evaluate the angle response of the sonic anemometer.

Windspeed measurements are taken along the transducer paths A,B and W. The horizontal transducers A and B have an angle of 120° relative to each other. The design is such that flow distortion is minimal when the sonic probe is turned into the wind. In the Speulderbos experiment the sonic-anemometer was not turned into the wind automatically. The turning was performed now and then depending on the importance of the measuring period. Consequently there are a lot of data in the data set were the angle ϕ between the mean wind direction DD and the sonic axis DD_S is larger then 30°, the angle above which significant deviations of the wind speed are to be expected. Here we seek to describe this angle response in a physical transparent way in order to be able to interpret calibration results and to correct 10 minute average values.

A transducer pair has a rotational symmetry axis going through the heart of the transducers. This suggest that the angle response of a single transducer pair without frame and boom can be described as a function of the angle of onflow and windspeed. Let θ be the angle of onflow relative to the transducer, where $\theta = 0$ is parallel to the transducer path. It may be expected that the response of the transducer to the component of the wind parallel to the transducer is highest when $\theta = 90°$ and gradually decrease when the angle of onflow becomes more parallel, due to shadowing effects. As long as the wind direction is well within the opening angle of the sonic we may ignore the mutual interference of the transducer pairs and the interference with the frame of the sonic. Thus for angles of onflow not to close to an azimuth 60° and elevations well below 45° say, we may expect that the whole response characteristic of the system can approximately determined from the angles of onflow θ_v (v = A, B or W) and the undisturbed windspeed U_r. We then define the response function $f_v(\theta_v,U_r)$ as:

$$U_v = U_r\cos(\theta_v)\cdot f_v(\theta_v,U_r) \tag{8.1}$$

The response function will be symmetric around $\theta = 0°$ and around $\theta = 90°$. Kaimal (1979) introduced a parametrisation of the transducer shadow function which fulfils these requirement. Here we use an adapted version for which the meaning of the parameters is more clear:

$$f(\theta) = a_0 - a_1\cdot\frac{e^{-a_2} - e^{-a_2\sin^2(\theta)}}{e^{-a_2} - 1} \tag{8.2}$$

It is easy to show that a_0 is the response value at $\theta = 90°$ and $a_0 - a_1$ is the response value at $\theta = 0°$. The parameter a_2 determines the angle at which half of the response change occurs. Windtunnel measurements are used to determine the parameters for each transducer pair at three wind speeds.

8.2 Windtunnel measurements

The sonic anemometer was calibrated following a method described by Kraan and Oost (1989). The calibration was performed for U_r = 6, 12 and 18 m s^{-1}. For each windspeed azimuth ranges from -90 to +90° in steps of 5° and elevation ranges from -22.5 to +22.5 in steps of 2.5°. At each position the three transducer wind speeds where measured and the angle of onflow θ_v was calculated.

Figure 8.1 shows the difference between the measured A-sensor windspeed and the free stream windspeed parallel to the A-sensor as a function of the angle of onflow. Free stream windspeed is U = 6 m s^{-1}. Shown are data for three different elevations. Data are corrected for the zero crossing jump described in a previous chapter. The most left points of each curve corresponds to azimuths of 60 and 55°. It is observed that the three curves coincide for all but these azimuths. For the azimuths larger then 50° apparently frame interference occur, making it impossible to correct measurements in this region with only transducer response functions.

Equation (8.2) is used for a regression analysis of the calibration data. It is extended with a fourth parameter which represents a possible offset. Data are corrected for the zero-crossing jump as described in chapter 2. Only data with azimuth between -50 and +50° are used. Table 8.a summarises the regression results for the three transducers pairs and for the three wind speeds. It is observed that the coefficients are not very sensitive for the windspeed. Significant differences occur between the different transducer pairs. Figure 8.2 shows the deviation of the cosine response for the A-sensor at U_r = 6 m s^{-1} as a function of the cosine of the angle of onflow. Also shown is the regression curve as given in Table 8.a.

It is observed that the fitt is reasonable over the whole range. Some remarks can be made however. The response of the sensor is not symmetric around θ = 90°. A significant improvement of the parametrisation can be made if we allow the orientation of the transducer to be varied in the regression. From this it is found that apparently the opening angle of the horizontal transducers A and B is not 120 but 124.5°. improving the standard deviation of the residuals from 5 to 4 cm s^{-1}. It seems that flow obstruction around the probe induces this apparent rotation. More pronounced is the result for the vertical sensor where a tilt of 0.7° out of the plane of symmetry of the probe is found. Figure 8.3 a and b show the regression results for a tilt of 0 and 0.7° respectively.

8.3 Comparison with field data

To investigate the consistency of the windtunnel results on the angle dependence of the sonic anemometer with in situ measurements we compared the sonic wind speed with the cup anemometer wind speed. Before comparing this measurements some precautions have to be made. Since the sonic was situated at 30 m height and the two neighbouring cup-anemometers at 24 and 31 m height respectively we used an interpolation scheme based on surface layer scaling to arrive at a cup-anemometer speed at 30 m. Time averaged cup anemometer measurements give the mean length of the wind vector or scalar wind, $<U_c>$. The averaging algorithm for the sonic windspeed was such that it produces the length of the mean windvector, $<U_c>$. Comparable wind speeds for both instruments can be derived by splitting wind speeds in mean values and fluctuations according to:

$$\begin{aligned} U_C(t) &= <U_C> + u_C'(t) \\ U_S(t) &= <U_S> + u_S'(t) \\ V_S(t) &= \quad\quad v_S'(t) \end{aligned} \tag{8.3}$$

Where U_C is the absolute windspeed, U_S is the longitudinal component of the windspeed and V_S the

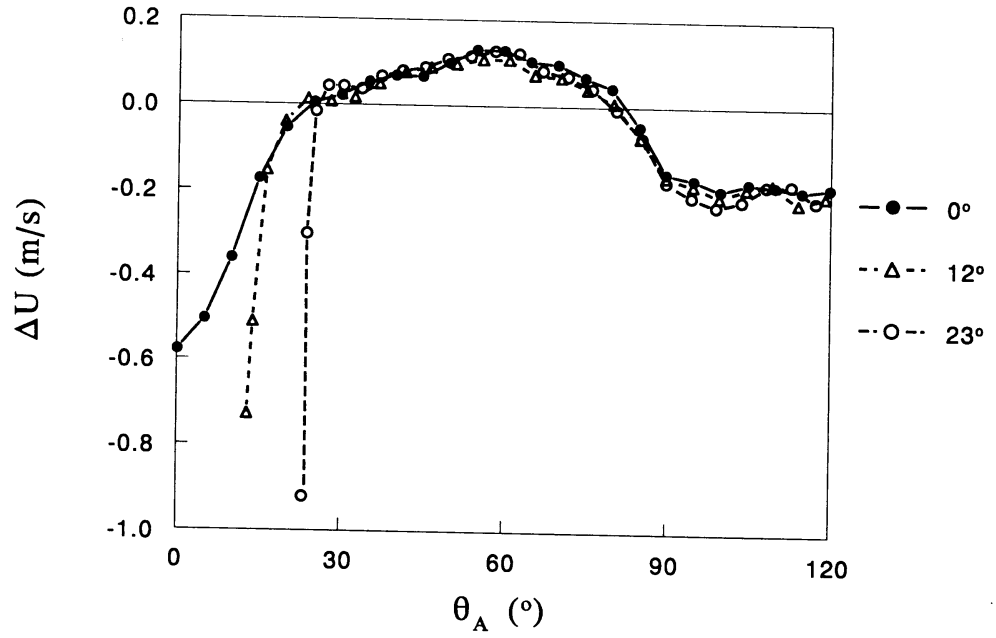

Figure 8.1 Response of one sonic-transducer (A-sensor) as a function of angle of onflow for three elevation.

transversal component of the windspeed. Since:

Uref (m/s)	sensor	offset (m/s)	a0	a1	a2	σ_v (m/s)
6	A	-0.123	1.072	0.090	2.6	0.04
12	A	-0.294	1.073	0.084	3.2	0.08
18	A	-0.509	1.069	0.089	3.9	0.12
6	B	0.020	1.083	0.131	1.1	0.05
12	B	-0.041	1.082	0.126	1.5	0.08
18	B	-0.019	1.079	0.129	1.9	0.11
6	W	0.017	1.042	0.189	(0.1)	0.04
12	W	0.107	1.077	0.285	(0.1)	0.09
18	W	0.158	1.072	0.297	(0.1)	0.13

Table 8.a Regression results for the three transducers of the sonic anemometer at three wind speeds

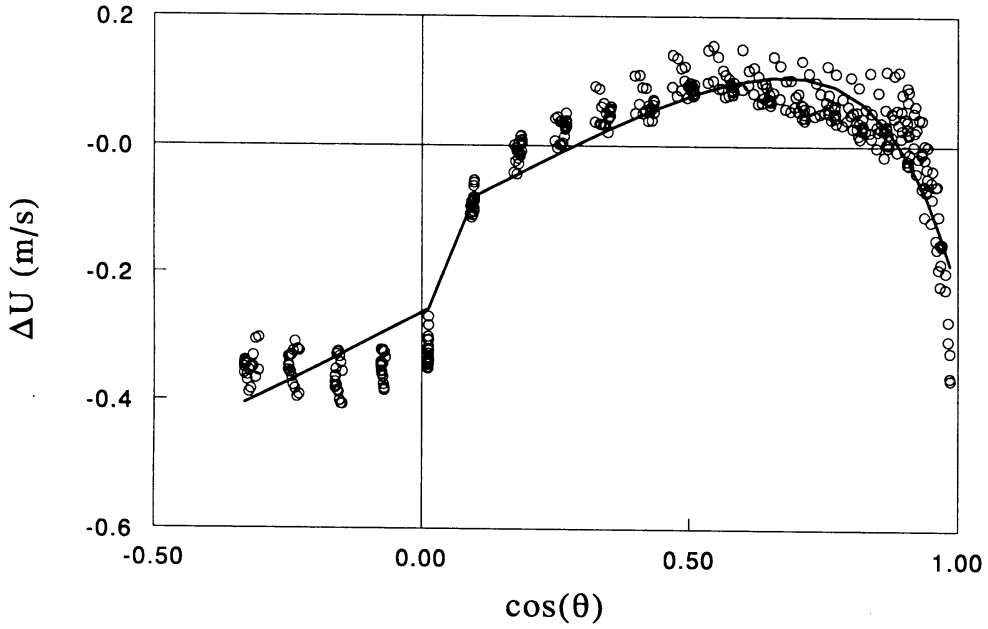

Figure 8.2 Response of one sonic-transducer (A-sensor) as a function of angle of onflow together with regression curve.

we find by substitution and averaging:

$$\langle U_C \rangle^2 + \sigma^2_{U_C} = \langle U_S \rangle^2 + \sigma^2_{U_S} + \sigma^2_{V_S} \qquad (8.5)$$

To investigate the response functions data were selected from the period 1 April to 31 December 1989 with windspeed at 36 m larger then 3 m s^{-1} and wind direction outside the interval (-45:45°) to avoid interference of the mast. To have a well defined angle of onflow data were selected with standard deviation of the wind direction less then 10°. Cup anemometer measurements were corrected for overspeeding (see appendix 11), but the small wind direction fluctuations implies only a small overspeeding correction. Figure 8.4a shows the sonic windspeed divided by the cup windspeed as a function of ϕ the angle of on flow relative to the sonic-frame. A significant angle response is observed. Figure 8.4b show response functions of the form defined by Equation (8.2) for the A-sensor and the B-sensor together with the same ratio as in Figure 8.4a but now with the sonic windspeed corrected for the angle response. The response functions were fitted on-eye, the coefficients are given in Table 8.b. The coefficients compare reasonable with the windtunnel results. The cup anemometers were calibrated in the KNMI windtunnel and the sonic anemometer was calibrated in the TNO-windtunnel. It is observed that the absolute wind speeds differ 2-3% in absolute science. A reason for this difference can be the unknown fill factor for the LUW-cup KNMI-windtunnel combination which was assumed to be equal to the larger KNMI-cup anemometer.

As observed by Grant and Wats (1989), the fluctuating wind direction within a 10 minute interval results in a response which is an average over the response functions. By the assumption of a tri-

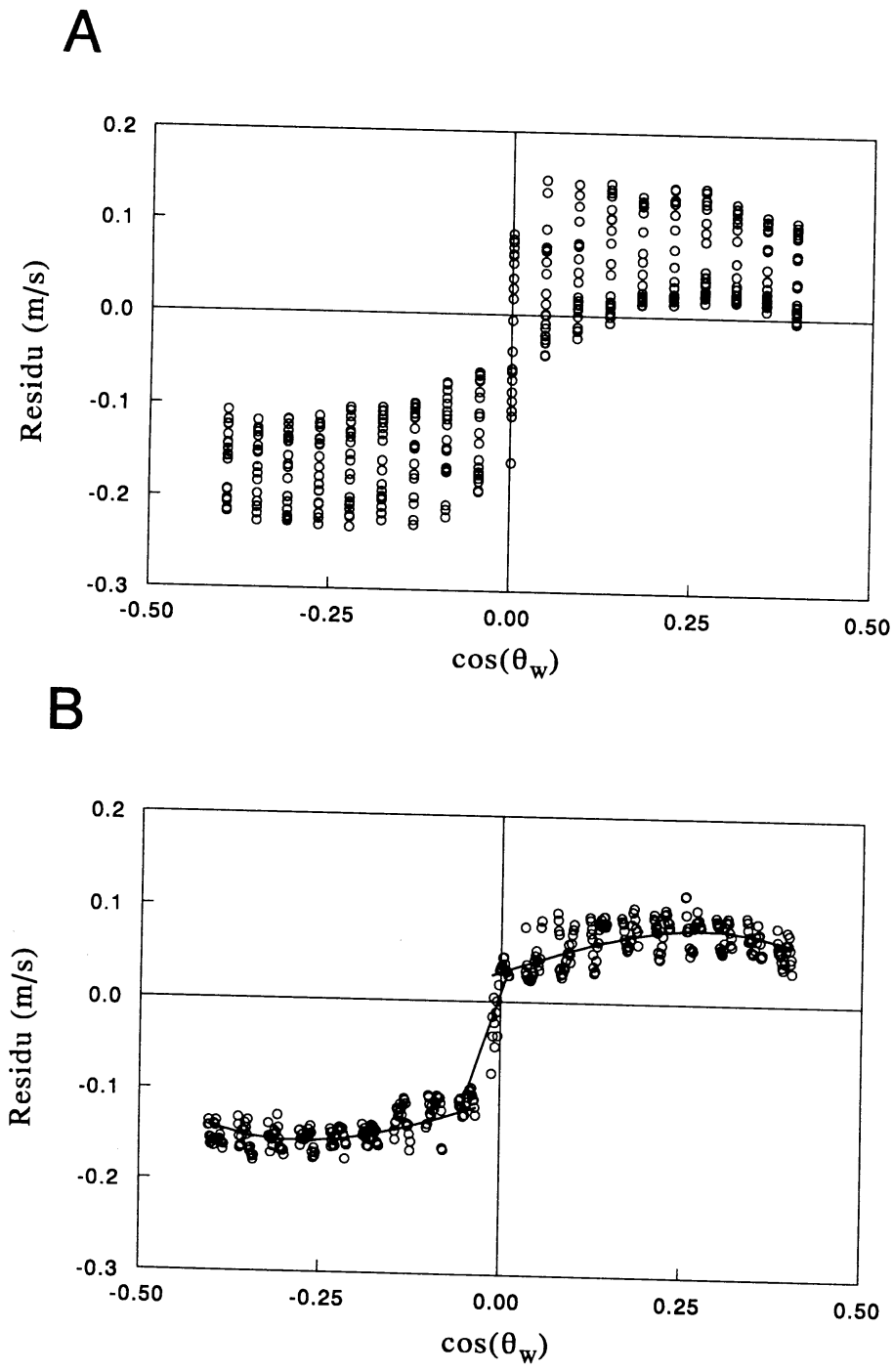

Figure 8.3 Response of one sonic-transducer (W-sensor) as a function of angle of onflow together with regression curve. A) without tilt, B) with tilt.

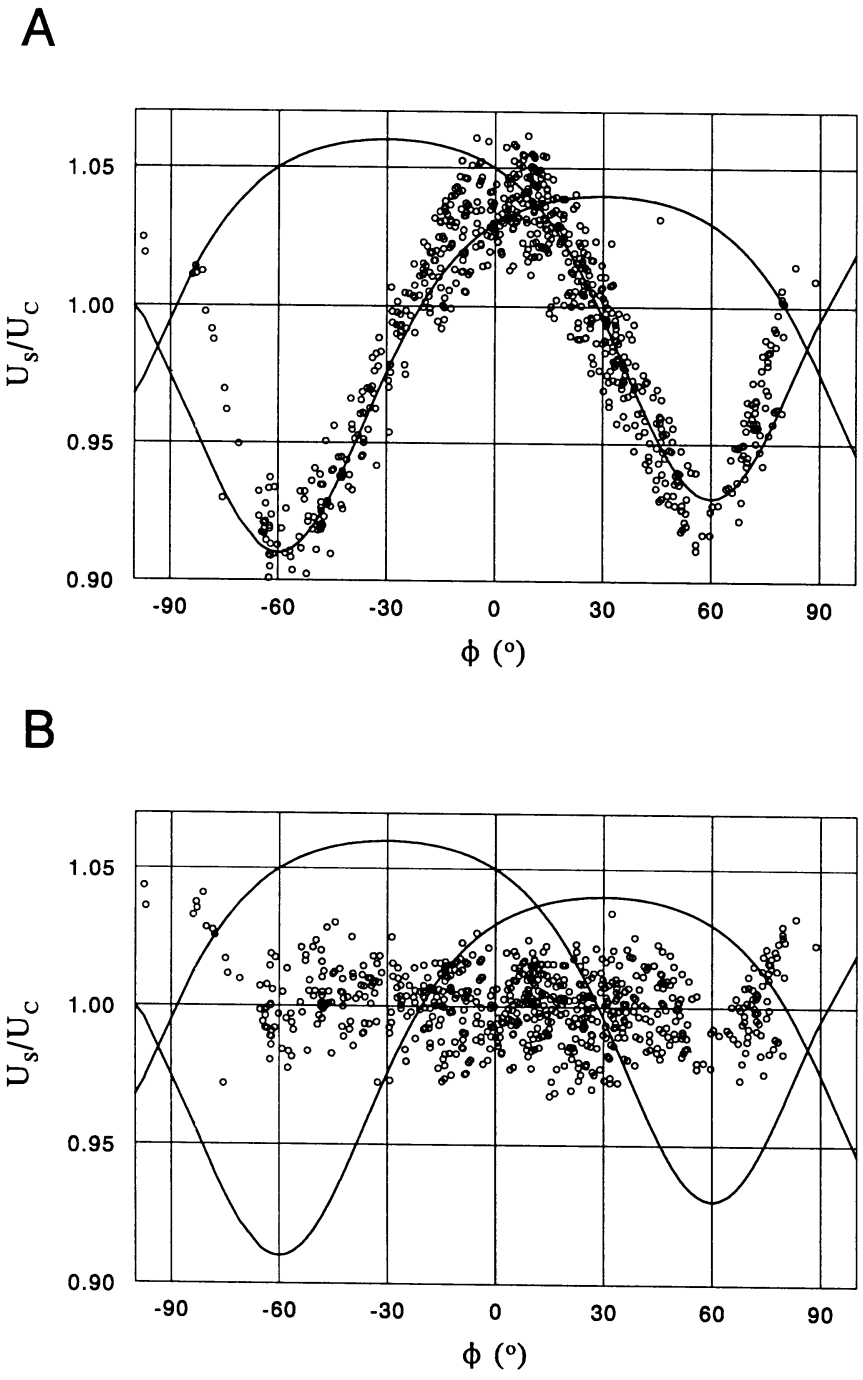

Figure 8.4 Sonic windspeed response as function of wind direction relative to sonic frame, a) uncorrected b) corrected with displayed response functions for A and B-sensor.

Gaussian distribution of the windvector it can be shown by a method described in Chapter 9 that for an average wind vector lying in the horizontal plane up to third order in the fluctuations the response is equal to the average over the response function values calculated for the wind vectors:
($U + \sigma_u$, $+\sigma_V$, $+\sigma_W$),
($U + \sigma_u$, $-\sigma_V$, $+\sigma_W$),
($U - \sigma_u$, $+\sigma_V$, $+\sigma_W$),
($U - \sigma_u$, $-\sigma_V$, $+\sigma_W$).

sensor	a0	a1	a2
A	1.06	0.13	2.5
B	1.04	0.13	2.5

Table 8.b Response function coefficients of on-eye fitt.

9 On the expectation value of functions of multi-dimensional Gaussian distributed random variables

In the practice of turbulence research it is often necessary to evaluate expectation values of functions of random variables (x). If the random variables obey a Gaussian distribution the integral can be approximated by Taylor expansion and evaluated straightforward. However, the necessity of evaluating the derivatives of the function can be a disadvantage. Here we develop a method to evaluate the integral by 2^N function evaluations at the corners of a cube centred around the mean value of x, where N is the dimension of the problem.

Let $f(x)$ be an analytic function from R^N to R, where x is a stochastic N-dimensional vector. We define the functional $G_A(f)$ as the average over the Gaussian distribution defined by **A**:

$$G_A(f) = \int dx^N e^{-\frac{1}{2}x\cdot A\cdot x} f(x) \tag{9.1}$$

where the integral is over the whole N-dimensional space, **A** is a N-dimensional symmetric positive definite matrix and the stochastic variable $\boldsymbol{x}$ has a zero mean value for this distribution. We can make a Taylor approximation on f around $\boldsymbol{x} = 0$:

$$f(x) = f(0)+\sum_i \partial_i f(0)\ x_i+\frac{1}{2}\sum_{i,j} \partial^2_{i,j} f(0)\ x_i x_j+\frac{1}{6}\sum_{i,j,k} \partial^3_{i,j,k} f(0)\ x_i x_j x_k+O(x^4) \tag{9.2}$$

and evaluate the integral for each term separately. It is observed that all the odd terms vanish due to the symmetry of the Gaussian function. There remains:

$$\langle f\rangle = f(0)+\frac{1}{2}\sum_{i,j} \partial^2_{i,j} f(0)\ R_{i,j}\sigma_i\sigma_j+O(\sigma^4) \tag{9.3}$$

where $R_{i,j}$ is the correlation coefficient for the variables x_i and x_j, and the σ's are the standard deviations of the components of the stochastic vector $\boldsymbol{x}$.

The problem now to be solved is to find for a fixed matrix **A** a set of P points $\{x_l\}$ in R^N and coefficients a_l such that for every function:

$$\sum_{l=1}^{P} a_l f(x_l) = \langle f\rangle + O(x^4) \tag{9.4}$$

Equation (9.4) itself can also be expanded in Taylor terms and subsequent terms can be equated to Equation (9.3):

$$\begin{aligned}\langle f\rangle = &\sum_{l=1}^{P} a_l f(0) + \sum_{l=1}^{P} a_l \sum_{i=1}^{N} x_{l,i}\partial_i f(0) + \frac{1}{2}\sum_{l=1}^{P} a_l \sum_{i,j=1}^{N} x_{l,i}x_{l,j}\partial^2_{i,j} f(0) + \\ &\frac{1}{6}\sum_{l=1}^{P} a_l \sum_{i,j,k=1}^{N} x_{l,i}x_{l,j}x_{l,k}\partial^3_{i,j,k} f(0) + O(x^4)\end{aligned} \tag{9.5}$$

If we choose a point $\boldsymbol{x}_1$ together with its reflected counterpart $-\boldsymbol{x}_1$ and asign the same coefficients to these points we see that with such a choice the odd terms corresponding to this points vanish. A particular convenient set are the point at the corners of the hyper cube centred around the origin, iven by $(\pm\sigma_1,\pm\sigma_2,....,\pm\sigma_N)$. Note that each point has its reflected counter part. With this selection of points the variance terms are also automatically fullfilled since the correlations R_{ii} are all 1. There remains the $N(N\text{-}1)/2$ co-variance terms and the zero order term to be equated. The number of free

parameters a_l is equal to the number of point pairs $Q = 2^{N-1}$. In order to have no over determined problem we should have:

$$Q = 2^{N-1} \geq \frac{N(N-1)}{2} + 1 \tag{9.6}$$

It is found that for N=1,2 and 3 the number of coefficients is equal to the number of equations to fulfil. For higher dimensions the problem becomes under-determined. For such case we can add extra constraints between the coefficients to make the problem well defined.

Here we present the solutions for $N = 3$ the case which of most interest for us. One point of each pair are listed.

points

$$\vec{p}_{1,2,3,4} = \begin{pmatrix} +\sigma_1 \\ +\sigma_2 \\ +\sigma_3 \end{pmatrix}, \begin{pmatrix} +\sigma_1 \\ +\sigma_2 \\ -\sigma_3 \end{pmatrix}, \begin{pmatrix} +\sigma_1 \\ -\sigma_2 \\ +\sigma_3 \end{pmatrix}, \begin{pmatrix} +\sigma_1 \\ -\sigma_2 \\ -\sigma_3 \end{pmatrix}$$

equations

$$\begin{aligned} a_1 + a_2 + a_3 + a_4 &= 1 \\ a_1 + a_2 - a_3 - a_4 &= R_{x,y} \\ a_1 - a_2 + a_3 - a_4 &= R_{x,z} \\ a_1 - a_2 - a_3 + a_4 &= R_{y,z} \end{aligned}$$

solution

$$\begin{aligned} a_1 &= \tfrac{1}{4}(1 + R_{x,y} + R_{x,z} + R_{y,z}) \\ a_2 &= \tfrac{1}{4}(1 + R_{x,y} - R_{x,z} - R_{y,z}) \\ a_3 &= \tfrac{1}{4}(1 - R_{x,y} + R_{x,z} - R_{y,z}) \\ a_4 &= \tfrac{1}{4}(1 - R_{x,y} - R_{x,z} + R_{y,z}) \end{aligned}$$

It is observed that the coefficients are expressed in terms of the correlation coefficients between the variables. When the function f has symmetries it is strait forward to diminish the number of calculations.

10 Mast interference

To investigate the influence of the mast on the wind measurements data were selected with angle of onflow less then 40°, windspeed larger then 3 m s^{-1} and standard deviation of the wind direction less then 10°. The latter selection criterium is imposed to avoid to much reliance on the overspeeding correction which will be discussed in paragraph 11 and to have a well defined angle of onflow relative to the mast. The two wind instruments are situated under slightly different angles relative to the mast. The sonic anemometer is at 165° and 2.8 m and the cup anemometer is at 174° and 2.5 m relative to the centre of the mast. Figure 10.1 shows the ratio of angle response corrected sonic windspeed and overspeeding corrected cup anemometer windspeed as a function of wind direction. It is observed that for wind direction in the interval (-30:+60°) serious deviations takes place. But even for the interval (60:180°) deviations of 1 to 2 percent are observed.
Noting that the cup anemometer and sonic anemometer positions relative to the mast are only slightly different one may wonder why the instrumental responses are so different for flow along the mast. A possible explanation is that cup anemometers are sensitive to horizontal windspeed gradients.

10.1 Sensitivity of cup anemometers for horizontal wind gradients

The balance of forces on a cup anemometer can be written schematically as:

$$\rho O D_+ (U-V_c)^2 - \rho O D_- (U+V_c)^2 = 0 \qquad (10.1)$$

where O is the cross section area of the cup, ρ is the density of air. U is the wind speed and V_c is the speed of the cup. D_+ and D_- are the drag coefficients for the open and closed side of the cup respectively. The first term is the drag force on the open side of the cup that moves with the wind, the second term the drag force on the closed side of the cup that moves against the wind.

Solving for V_c gives:

$$V_c = \frac{D_+ - D_-}{D_+ + D_-} \cdot U = p \cdot U \qquad (10.2)$$

From the calibration result and geometry (Bosveld et al., 1998) we find for the LUW cup anemometers $p = 0.3$.

Let $U_c = V_c/p$ be the windspeed given by the cup anemometer at an actual windspeed of U when no gradient is present. Let ΔU the horizontal windspeed difference over the diameter of the cup anemometer, ΔU positive for larger windspeed at the open cup side. We then have for the force balance:

$$D_+ \left(U + \frac{1}{2}\Delta U - \frac{1}{p}(U_c + \Delta U_c) \right)^2 = D_- \left(U - \frac{1}{2}\Delta U + \frac{1}{p}(U_c + \Delta U_c) \right)^2 \qquad (10.3)$$

where ΔU_c is the bias in cup anemometer windspeed. From this it is immediately clear that $\Delta U_c = 1/(2p)\ \Delta U$. This gives for the LUW-cup anemometer a bias of 1.7 times the windspeed difference over the cup anemometer.

parameters a_l is equal to the number of point pairs $Q = 2^{N-1}$. In order to have no over determined problem we should have:

$$Q = 2^{N-1} \geq \frac{N(N-1)}{2} + 1 \tag{9.6}$$

It is found that for N=1,2 and 3 the number of coefficients is equal to the number of equations to fulfil. For higher dimensions the problem becomes under-determined. For such case we can add extra constraints between the coefficients to make the problem well defined.

Here we present the solutions for $N = 3$ the case which of most interest for us. One point of each pair are listed.

points

$$\vec{p}_{1,2,3,4} = \begin{pmatrix} +\sigma_1 \\ +\sigma_2 \\ +\sigma_3 \end{pmatrix}, \begin{pmatrix} +\sigma_1 \\ +\sigma_2 \\ -\sigma_3 \end{pmatrix}, \begin{pmatrix} +\sigma_1 \\ -\sigma_2 \\ +\sigma_3 \end{pmatrix}, \begin{pmatrix} +\sigma_1 \\ -\sigma_2 \\ -\sigma_3 \end{pmatrix}$$

equations

$$\begin{aligned} a_1 + a_2 + a_3 + a_4 &= 1 \\ a_1 + a_2 - a_3 - a_4 &= R_{x,y} \\ a_1 - a_2 + a_3 - a_4 &= R_{x,z} \\ a_1 - a_2 - a_3 + a_4 &= R_{y,z} \end{aligned}$$

solution

$$\begin{aligned} a_1 &= \tfrac{1}{4}(1 + R_{x,y} + R_{x,z} + R_{y,z}) \\ a_2 &= \tfrac{1}{4}(1 + R_{x,y} - R_{x,z} - R_{y,z}) \\ a_3 &= \tfrac{1}{4}(1 - R_{x,y} + R_{x,z} - R_{y,z}) \\ a_4 &= \tfrac{1}{4}(1 - R_{x,y} - R_{x,z} + R_{y,z}) \end{aligned}$$

It is observed that the coefficients are expressed in terms of the correlation coefficients between the variables. When the function f has symmetries it is strait forward to diminish the number of calculations.

11 Cup anemometer overspeeding corrections

11.1 Introduction

The cup anemometer is normally used to measure an average over a certain time interval of the length of the horizontal wind speed vector. However, the cup anemometer is not an ideal instrument. When exposed to a variable wind as is the normal situation in the atmosphere a cup anemometer overestimates the average wind speed. This overspeeding occurs because the time constant of the instrument for adaption to a changing windspeed is inversely proportional to the windspeed. It is therefor common to use a distance constant l_0 to describe the aspects of the dynamical behaviour. A step of increasing windspeed is more quickly followed by the measuring device then a step of decreasing wind speed. A second cause of overspeeding is the influence of the vertical wind on the cup rotation speed. The drag that cup experience depends on the direction of onflow and is influenced by wake interference of the other cups in the configuration. For pure horizontal winds the cups of the instrument resides partly in each others wake. When a vertical wind is present the cups come out of the wake and experience a different drag force. Experimental results indicate that this drag increase is more profound on the open side of the cup then on the closed side. Consequently the instrument overestimates the horizontal wind in the presence of vertical velocity fluctuations. In this section the theory of cup anemometer overspeeding will be described and the consequences for the measurements will be discussed.

11.2 Cup anemometer dynamics

A general treatment of cup anemometer dynamics is given by Wyngaard at al. (1973). They show that the system can be described by 8 parameters which fulfil several constraints. Coppin (1982) determined these parameters for several different types of cup anemometers. Kristensen (1993) gives an excellent review of the problem and show the simplification that can be made for surface layer turbulence. Here we follow his work.

The relative overspeeding is to a good approximation given by:

$$\delta = \frac{l}{l+\Lambda}\frac{1}{U^2}\int_{-\infty}^{+\infty}\frac{k^2 l_0^2}{1+k^2 l_0^2}F_U(k)dk + \frac{\mu_2}{2}\frac{\sigma_w^2}{U^2} \qquad (11.1)$$

where:

Λ	A length scale which is small,
l_0	response length,
U	windspeed,
μ_2	coefficient characterising the discrepancy from the elevation the cosine response,
σ_w^2	variance of the vertical wind,
$F_U(k)$	longitudinal wind spectrum in wave number domain,
k	wave number.

Here some smaller effects are ignored of which the most important are stress bias and bias due to asymmetric elevation response. Kristensen (1993) shows that under normal surface layer conditions and normal instruments these effects are small relative to those described in Equation (11.1).

The first term on the r.h.s of Equation (11.1) is the u-bias. It shows that the instruments bias is

determined by the high frequency part of the spectrum and the response length of the instrument sets the length scale below which fluctuations are not followed well by the instrument and contribute to the overspeeding. The second term is proportional to the vertical velocity variance and contains no dynamic response characteristics of the instrument.

Spectral characteristics of the horizontal wind in the roughness-layer

The spectrum of the horizontal wind is a more difficult subject. Of course the spectra in the surface layer of the atmosphere are well described in the literature (Kaimal et al., 1972). But spectra for the roughness layer are scarce. Here we assume that the turbulence has an inertial subrange extending to scale larger then the response length of the cup anemometer. Moreover it is assumed that the turbulence is isotropic in this spectral region. These assumptions are justified to some extend in the chapter about structure parameters of the vertical wind.

In the inertial subrange the spectrum F_u is given by:

$$F_u(k) = \frac{1}{2}\alpha_1 \varepsilon^{2/3} |k|^{-5/3} \tag{11.2}$$

where ε is the energy dissipation rate and α_1 is the Kolmogorov constant for the longitudinal spectrum. If an inertial range exists we can substitute this formula into Equation (11.1) and integrate to arrive at:

$$\delta = \frac{\pi}{\sqrt{3}}\alpha_1 \frac{l}{l+\Lambda}\frac{(\varepsilon l_0)^{2/3}}{U^2} + \frac{\mu_2}{2}\frac{\sigma_w^2}{U^2} \tag{11.3}$$

The dissipation can be estimated from the structure parameter of the vertical wind through the relation:

$$C_w^2 = 4.01\alpha_1 \varepsilon^{2/3} \tag{11.4}$$

Combining this last two equation gives the overspeeding in relatively easy measurable quantities:

$$\delta = 4.01\frac{\pi}{\sqrt{3}}\frac{l}{l+\Lambda}\frac{C_w^2 \cdot l_0^{2/3}}{U^2} + \frac{\mu_2}{2}\frac{\sigma_w^2}{U^2} \tag{11.5}$$

Thus to estimate the overspeeding of a cup anemometer at a certain level in the profile we need to know at that level the windspeed, the variance of the vertical wind and its structure parameter.

11.3 Scaling laws of σ_w and C_w^2

The variance and structure parameter of the vertical wind speed are measured at one level (30 m). To perform the overspeeding correction for other levels in the wind profile we have to rely on scaling relations for these quantities. Above the roughness layer Monin-Obhukov similarity theory apply. For this correction procedure we shall assume that the same relations hold in the roughness layer.

For the variance of the vertical wind Panofsky and Dutton (1984) recommend:

$$\frac{\sigma_w^2}{u_*^2} = 1.56\left(1-3\frac{z}{L}\right)^{2/3} \quad \frac{z}{L}<0$$
$$\frac{\sigma_w^2}{u_*^2} = 1.56 \qquad \frac{z}{L}>0 \tag{11.6}$$

where z is the height above the displacement height. The structure parameter scales according to:

$$\frac{C_w^2 z^{2/3}}{u_*^2} = f(z/L) \tag{11.7}$$

This shows that even for neutral conditions there is a height dependence. This makes the influence of the two terms in the overspeeding correction for wind difference measurement different. The stability function for C_w^2 is derived in Chapter ?. From these relation and given eddy correlation measurements on the 30 m level we can now derive the corresponding values for the levels in the wind profile.

11.4 Dynamical cup model

To get confidence in the overspeeding estimates described above we applied a dynamical model of the cup anemometer to a 5 Hz sample registration of 15 days of sonic anemometer data. This is the model described by Kristensen (1993) from which he derives his expressions for overspeeding. Comparing the output of the cup model with the original sonic anemometer signal gives us the model based overspeeding for roughness layer turbulence conditions. Instrumental characteristics are taken from Bosveld et al.(1998). The response length l_0 is 1.4 m and the tilting parameter μ_2=1.0. Figure 11.1 shows the dynamical cup model overspeeding versus the overspeeding calculated on the basis of Equation (11.5).

11.5 Overspeeding derived from field data

A more rigorous validation of the correction procedure is obtained by comparing angle corrected sonic windspeed measurements with cup anemometer readings. It may seem that some cyclic dependency occur here since overspeeding corrected cup anemometer data are used in deriving the angle dependency correction of the sonic anemometer. Indeed it is a iterative process to arrive at the results, but to avoid this cyclic dependency as much as possible here only sonic anemometer data are used with angle of onflow less then 30°, this ensures that corrections for angle response are small. In the derivation of the angle response of the sonic anemometer only cup anemometer data were used with standard deviation of wind direction less then 10°, ensuring that overspeeding corrections were small in that case.

From Figure 10.1 it is observed that only for with wind direction between 180 and 250° the mast and boom interference is small and constant. Thus only data within this wind direction sector were accepted. In this subset data with wind direction standard deviation smaller then 10° where used to obtained a linear regression between sonic and cup anemometer windspeed. This regression was applied to all sonic anemometer readings in the subset.

Figure 11.2 shows the measured overspeeding, i.e. the difference between uncorrected cup anemometer values and sonic wind speeds, versus the modelled overspeeding, i.e. the difference between uncorrected and corrected cup anemometer wind speeds. It is observed that the measured overspeeding is slightly smaller (12% on the average) then the modelled overspeeding. This 12% amounts to approximately 1% difference in terms of windspeed result. In the light of the

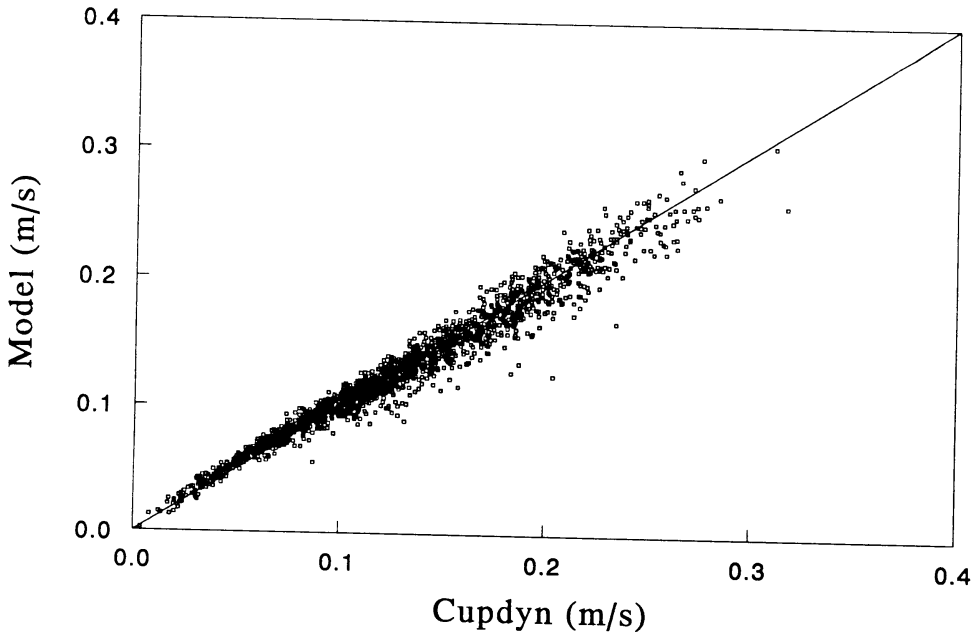

Figure 11.1 Overspeeding estimated from a dynamical cup anemometer model versus the overspeeding estimated from σ_w and C_w^2.

instrumental limitation this result seems to confirm the correctness of the proposed overspeeding correction procedure. What remains is the uncertainty about the scaling behaviour of σ_w and C_w^2 in the roughness layer.

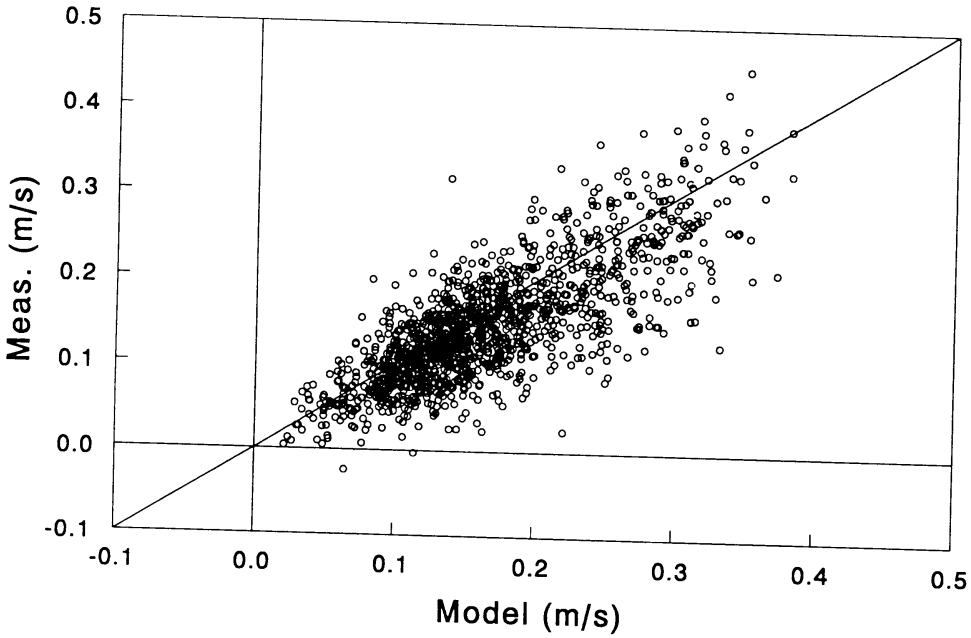

Figure 11.2 Measured overspeeding as function of modelled overspeeding.

Literature

Andreas E. L. (1981). The effects of volume averaging on spectra measured with Lyman-Alpha hygrometer. J. Appl. Meteorol., 20, 467-475.

Anselmet F., Y. Gagne, E. J. Hopfinger and R. A. Antonia (1984). High-order velocity structure functions in turbulent shear flow. J. Fluid Mech., 140, 63-89.

Bosveld F. C., J. G. van der Vliet and W. A. A. Monna (1998). The KNMI Garderen experiment, Micro-meteorological observations 1988-1989, instruments and data set. KNMI Technical Report TR-208. De Bilt, The Netherlands.

Brutsaert W. (1975). On a derivable formula for longwave radiation from clear skies. Water Resources Research, 11, 742-744.

Coppin P. A. (1982). An examination of cup anemometer overspeeding. Meteorol. Rdsch., 35, 1-11.

De Jong J. B. R. M. (1980). Een karakterisering van de zonnestraling in Nederland, met bijlage. TU-Eindhoven, Afstudeerverslag. (In Dutch).

Fairall C. W., J. B. Edson, S. E. Larsen and P. G. Mestayer (1990). Inertial-Dissipation air-sea flux measurements: a prototypoe system using realtime spectral computations. J. Atmos. Ocean. Technol., 7, 425-453.

Frisch U, P. L. Sulem and M. Nelkin (1978). A simple dynamical model of intermittent fully developed turbulence. J. Fluid Mech., 87, 719-736.

Grant A. L. M. and R. D. Watkins (1989). Errors in turbulence measuremetns with a sonic anemometer. Boundary-Layer Meteorol., 46, 181-194.

Halldin S. and A. Lindroth (1992). Errors in net radiometry. Comparison and evaluation of six radiometer designs. J. Atmos. Ocean. Technol., 9, 762-783.

Hanafusa T., T. Fujitani, Y. Kobori and Y. Mitsuta (1982). A new type sonic anemometer-thermometer for field operation. Papers in Meteorology and Geophysics, 33, 1, 1-19.

Hinze J. O. (1959). Turbulence. Mc Graw-Hill, New York.

Kaimal J. C., J. C. Wyngaard and D. A. Haugen (1968). Deriving power spectra from a three-component sonic anemometer. J. Appl. Meteorol., 7, 827-837.

Kaimal J. C., J. C. Wyngaard, Y. Izumi and O. R. Cote (1972). Spectral characteristics of surface layer turbulence. Q. J. R. Meteorol. Soc., 98, 563-589.

Kaimal J. C. (1979). Sonic anemometer measurement of atmospheric turbulence. Proceedings of the dynamic flow conference, I. M. S. T., Marseille, France, September 11-14, 1978 and Johns Hopkins University, Baltimore, USA, Septenber 18-21, 1978. Proceedings of the Dynamic Flow Conference 1978, P. O. Box 121, DK-2740, Skovlunde, Denmark.

Kohsiek W. (1982). Measuring CT2, CQ2 and CTQ in the unstable surface layer, and relations to the vertical fluxes of heat and moisture. Boundary-Layer Meteorol., 24, 89-107.

Kohsiek W. (1984). Inertial subrange correlation between temperature and humidity fluctuations in the unstable surface layer above vegetated terrains. Boundary-Layer Meteorol., 29, 211-224.

Kohsiek W. and F. C. Bosveld (1987). Heat and moisture fluxes and related structure parameters in the unstable atmospheric surface layer over short vegetations. KNMI Scientific Report, WR-87-7, De Bilt, The Netherlands.

Kohsiek W. (1996). On the KNMI calibration of net radiometers. KNMI Technical report, TR-189. De Bilt, The Netherlands.

Kolmogorov A. N., (1962). A refinement of previous hypothesis concerning the local structure of turbulence in a viscous incompressible fluid at high Reynolds number. J. Fluid Mech., 13, 82-85.

Kraan C. and W. A. Oost (1989). A new way of anemometer calibration and its application to a sonic anemometer. J. Atmos. Ocean. Technol., 6, 516-524.

Kristensen L. and D. R. Fitzjarrald (1984). The effect of line averaging on scalar flux measurements with a sonic anemometer near the surface. J. Atmos. Ocean. Technol., 1, 138-146.

Kristensen L. (1993). The cup anemometer and other exciting instruments. Thesis Technical University of Denmark. Risø-R-615(EN). Risø, Roskilde.

Lumley J. L. and H. A. Panofsky (1964). The structure of atmospheric turbulence. Wiley Interscience, New York, 239pp.

Lumley J. L. (1965). Interpretation of time spectra measured in high-intensity shear flows. The physics of fluids, 8, 1056-1062.

Moore C. J. (1986). Frequency response corrections for eddy correlation systems. Boundary-Layer Meteorol., 37, 17-35.

Obhukov A. M., (1962). Some specific features of atmospheric turbulence. J. Fluid Mech., 13, 77-81.

Panofsky H. A. and J. A. Dutton (1984). Atmospheric turbulence. Wiley and Sons, Inc, USA.

Raaf W. R. (1987). De maximale globale straling bij onbewolkt weer. KNMI Memo FM-87-21. Unpublished manuscript. (In Dutch).

Rice S. O. (1945). Mathematical analysis of random noise. Bell. Syst. Technol. J., 24, 46-156.

Tatarski V. I. (1967). Wave propagation in a turbulent medium. Dover, New York.

Van der Ploeg R. (1995). Measurements of the structure parameter of vertical wind-velocity in the atmospheric boundary layer. KNMI Technical Report, TR-173. De Bilt, The Netherlands.

Velds C. A. (1992). Zonnestraling in Nederland. Thieme, Baarn, 170pp.

Weil A. (1991). Indirect meaurements of fluxes using Doppler sodar. In: Land surface evaporation, measurements and parametrization, eds. T. J. Schmugge and J.-C. André. Springer Verlag, 301-312.

Wyngaard J. C., J. T. Bauman and R. A. Lynch (1973). Cup anemometer dynamics. Proc. Instr. Soc. of America (Pittsburg), 1, 701-708.

Wyngaard J. C. and S. Zhang (1985). Tranducer-shadow effects on turbulence spectra measured by sonic anemometers. J. Atmos. Ocean. Technol., 2, 548-558.

Wyngaard J. C. and S. F. Clifford (1977). Taylor's hypothesis and high-frequency turbulence spectra. Journal of the Atmopheric Sciences, 34, 922-929.